JOURNAL OF GEOPHYSICAL RESEARCH, VOL. 115, D00J04, doi:10.1029/2009JD013073, 2010

Planning, implementation, and first results of the Tropical Composition, Cloud and Climate Coupling Experiment (TC4)

Owen B. Toon,[1] David O. Starr,[2] Eric J. Jensen,[3] Paul A. Newman,[2] Steven Platnick,[2] Mark R. Schoeberl,[2,4] Paul O. Wennberg,[5] Steven C. Wofsy,[6] Michael J. Kurylo,[7] Hal Maring,[8] Kenneth W. Jucks,[8] Michael S. Craig,[3] Marilyn F. Vasques,[3] Lenny Pfister,[3] Karen H. Rosenlof,[9] Henry B. Selkirk,[7] Peter R. Colarco,[2] Stephan R. Kawa,[2] Gerald G. Mace,[10] Patrick Minnis,[11] and Kenneth E. Pickering[2]

Received 24 August 2009; revised 18 February 2010; accepted 2 March 2010; published 15 July 2010.

[1] The Tropical Composition, Cloud and Climate Coupling Experiment (TC4), was based in Costa Rica and Panama during July and August 2007. The NASA ER-2, DC-8, and WB-57F aircraft flew 26 science flights during TC4. The ER-2 employed 11 instruments as a remote sampling platform and satellite surrogate. The WB-57F used 25 instruments for in situ chemical and microphysical sampling in the tropical tropopause layer (TTL). The DC-8 used 25 instruments to sample boundary layer properties, as well as the radiation, chemistry, and microphysics of the TTL. TC4 also had numerous sonde launches, two ground-based radars, and a ground-based chemical and microphysical sampling site. The major goal of TC4 was to better understand the role that the TTL plays in the Earth's climate and atmospheric chemistry by combining in situ and remotely sensed data from the ground, balloons, and aircraft with data from NASA satellites. Significant progress was made in understanding the microphysical and radiative properties of anvils and thin cirrus. Numerous measurements were made of the humidity and chemistry of the tropical atmosphere from the boundary layer to the lower stratosphere. Insight was also gained into convective transport between the ground and the TTL, and into transport mechanisms across the TTL. New methods were refined and extended to all the NASA aircraft for real-time location relative to meteorological features. The ability to change flight patterns in response to aircraft observations relayed to the ground allowed the three aircraft to target phenomena of interest in an efficient, well-coordinated manner.

Citation: Toon, O. B., et al. (2010), Planning, implementation, and first results of the Tropical Composition, Cloud and Climate Coupling Experiment (TC4), *J. Geophys. Res.*, *115*, D00J04, doi:10.1029/2009JD013073.

1. Introduction

[2] The Tropical Composition, Cloud and Climate Coupling Experiment (TC4) was based in Costa Rica and Panama during July and August 2007. The more than 600 participants came from multiple NASA centers, NOAA, and NCAR, as well as numerous universities and private research institutions in the United States, Panama and Costa Rica. The field mission involved the NASA DC-8, ER-2 and WB-57F aircraft (Figure 1) as well as ground-based instruments and sondes. The mission was aimed at better understanding the tropical tropopause layer (TTL) by combining in situ and remotely sensed data from the ground, balloons, and aircraft with data from NASA satellites such as Aura, CloudSat, CALIPSO, Aqua, and Terra. The TTL is the gateway to the stratosphere. It is of critical importance to the Earth's climate and atmospheric chemistry because it controls the entry to the stratosphere of greenhouse gases such as water vapor, and a

[1]Department of Atmospheric and Oceanic Sciences and Laboratory for Atmospheric and Space Physics, University of Colorado at Boulder, Boulder, Colorado, USA.
[2]Laboratory for Atmospheres, NASA Goddard Space Flight Center, Greenbelt, Maryland, USA.
[3]Earth Sciences Division, NASA Ames Research Center, Moffett Field, California, USA.
[4]Polar Office, Science and Technology Corporation, Columbia, Maryland, USA.
[5]Division of Engineering and Applied Sciences and Division of Geological and Planetary Sciences, California Institute of Technology, Pasadena, California, USA.
[6]Department of Earth and Planetary Sciences, Harvard University, Cambridge, Massachusetts, USA.
[7]Goddard Earth Sciences and Technology Center, University of Maryland Baltimore County, Baltimore, Maryland, USA.
[8]Earth Sciences Division, NASA, Washington, D. C., USA.
[9]Earth System Research Laboratory, NOAA, Boulder, Colorado, USA.
[10]Department of Atmospheric Sciences, University of Utah, Salt Lake City, Utah, USA.
[11]Science Directorate, NASA Langley Research Center, Hampton, Virginia, USA.

0148-0227/10/2009JD013073

Figure 1. Early morning on 5 August 2007 at the Juan Santamaria International Airport in Costa Rica. From left to right, NASA's DC-8, WB-57F, and ER-2 prepare for a flight. In the background a large mesoscale convective complex in the Pacific Ocean near Costa Rica rises into the tropopause transition layer. The aircraft investigated this feature for several hours, until it dissipated. Photo by Sean Davis.

multitude of gases of importance to ozone chemistry. Deep convection sometimes penetrates the TTL to reach the stratosphere, while gentle upward motions within the TTL may also loft materials across the tropical tropopause. Hence the chemistry of the stratosphere, including the global ozone budget, may be affected in a significant way by processes that alter the transport across the TTL and by the chemicals in the TTL. Changes in water vapor in the stratosphere and upper troposphere can play an important role in modulating the climate since water is the most powerful greenhouse gas in the atmosphere. *Soden et al.* [2008] show that the maximum sensitivity of surface temperature to water vapor changes occurs in the tropical upper troposphere. Radiative transfer calculations also suggest that small changes in stratospheric humidity have important impacts on the earth's radiation budget [e.g., *Forster and Shine*, 2002]. The TTL is the main dehydration region for air entering the stratosphere, and it is also an important reservoir for moisture lofted by tropical convection. Understanding how water behaves in the TTL is one key to better understanding the greenhouse effect and global climate change. The TTL also contains cirrus clouds. One type of cirrus consists of anvils, the flattened tops of tropical cumulus clouds. In just a few minutes, a cumulus cloud can pump vast quantities of air from near the tropical surface to the TTL, where the air spills out into the anvils. The TTL also contains cirrus clouds that form in situ. Some of these are so thin that they cannot be seen with the naked eye, and so are called subvisible cirrus. These clouds are easily detected by some satellites, however, and are now known to cover a large fraction of the tropics.

[3] Here we provide an overview of the TC4 mission. We first describe the goals for TC4. We then discuss the instrument packages on the aircraft and other platforms. Next, we summarize the various flights that were conducted. Finally, we provide an overview of the results from TC4 to date.

2. Scientific Motivation

[4] Table 1 lists the major questions that TC4 sought to address. The focus of TC4 was the TTL. However, TC4 recognized that an understanding of the flux of material into the TTL requires constituent measurements throughout the troposphere, including convectively disturbed regions. An understanding of the role of water vapor and ozone in the climate system requires observations below the lower boundary of the TTL in the free troposphere. Similarly, measurements in the lower stratosphere are required to understand how processes in the TTL influence humidity and other properties of the stratosphere. Below we address a number of issues related to the questions in Table 1.

2.1. Definition of the TTL

[5] A number of workers have noted that the layer of the tropical atmosphere between about 12 km altitude (pressure~200 hPa, potential temperature, θ, ~350 K) and the cold point tropopause (16–17 km, 100–90 hPa, $\theta \sim 380$ K) has characteristics intermediate between those of the troposphere and stratosphere [e.g., *Highwood and Hoskins,* 1998; *Thuburn and Craig,* 2002; *Fueglistaler et al.*, 2009]. This layer was referred to as the substratosphere by Thuburn and Craig. The cold point tropopause (altitude of the temperature minimum) is important for understanding stratospheric dehydration, and for infrared radiative forcing. However, it does not mark a discontinuity in tracer fields. In fact, some tropospheric circulations (such as overshooting convection, monsoon circulations, and equatorial waves) can extend for some distance above the cold point tropopause. Thus, it seems appropriate to extend the definition of the transition layer between the tropical troposphere and stratosphere to include the first few kilometers above the cold point. Therefore this region is referred to as the tropical tropopause layer (TTL) rather than the substratosphere. The TTL as defined here includes the entire region between the level at which the temperature profile begins to depart from the moist adiabatic profile enforced by tropospheric convection (~12 km in convectively active regions [*Gettelman and Forster,* 2002]) to the level in the stratospheric overworld beyond which the influence of tropospheric circulations becomes insignificant (~50 hPa, ~20 km, θ ~470 K). The stratospheric overworld is defined to be the volume of the stratosphere with potential temperature above the tropical tropopause potential temperature, θ~380 K. At middle latitudes there is a lower stratosphere with potential temperatures characteristic of the tropical troposphere [*Holton et al.*, 1995].

Table 1. Major Questions Addressed by TC4

Question Number	Scientific Question
1	What mechanisms maintain the humidity of the stratosphere? What are the relative roles of large-scale transport and convective transport and how are these processes coupled?
2	What are the physical mechanisms that control (and cause) long-term changes in the humidity of the upper troposphere in the tropics and subtropics?
3	What controls the formation, maintenance and distribution of thin cirrus in the TTL, and what is the influence of thin cirrus on radiative heating and cooling rates, and on vertical transport?
4	What are the chemical fates of short-lived compounds transported from the tropical boundary layer into the TTL? (i.e., what is the chemical boundary condition for the stratosphere?)
5	What are the mechanisms that control ozone within and below the TTL? What is the chemical nature of the outflow from convective regions?
6	How do convective intensity and aerosol properties affect cirrus anvil properties?
7	How do cirrus anvils, and tropical cirrus in general, evolve over their life cycle? How do they impact the radiation budget and ultimately the circulation?
8	How can space-based measurements of geophysical parameters, particularly those known to possess strong variations on small spatial scales (e.g., H_2O, cirrus), be validated in a meaningful fashion?

[6] Within the TTL, as defined above, a number of parameters undergo rapid change in the vertical. For example, in the lower portion of the TTL (~12–14 km) convective mass fluxes (and clear-sky radiative cooling rates) decrease rapidly with height, corresponding to the region of the main convective outflow. The annual mean convective mass flux out of the boundary layer between 15°N and 15°S is about 3.0×10^{11} kg/s, and about 50% of this mass flux from the boundary layer typically reaches the lowermost of the TTL (12–13 km). However, the annual flux across the 100 hPa surface (near the cold point) is only about 10^{10} kg/s, which is only ~3% of the flux of air out of the tropical boundary layer [*Rosenlof and Holton,* 1993]. There are also vertical variations in the horizontal transport, and above 14 km, where convective transport and mixing are small, large-scale horizontal transport processes become increasingly important for meridional transport and mixing of trace constituents. A layer extending from approximately 15.5 km into the lowermost stratosphere is (at least in clear-sky conditions) radiatively heated [*Gettelman et al.*, 2004]. In balance with this heating, air in this layer must be ascending and will ultimately end up in the stratosphere. As a result, the composition of the TTL represents a lower boundary condition for important trace gases that affect stratospheric ozone, including water vapor, HO_x and NO_x species, and halogens. The TTL is also a region in which relative humidity increases with altitude, with a maximum at the tropopause [*Vömel et al.*, 2002].

[7] In addition, while it is known that photochemistry within the TTL leads to rapid ozone production, the interplay of the convective processes (that transport short-lived compounds that fuel ozone production from the lower troposphere), in situ photochemistry, and large-scale dynamics remains poorly constrained.

[8] The transport and transformations within the TTL are also important for understanding the fate of compounds transported into the tropical upper troposphere and the chemical boundary condition for the stratosphere. The above estimates of mass fluxes indicate that only a small fraction of the air leaving the tropical boundary layer actually crosses into the tropical stratosphere. For short-lived or soluble constituents, the fraction reaching the stratosphere will be even smaller. However, these estimates are very uncertain and the flux of compounds into the stratosphere will depend on the precise balance of different physical and chemical processes in the TTL. Better quantification of these processes is essential for establishing the chemical boundary condition for the stratosphere, and understanding how this will change.

2.2. TTL Water Vapor Budget

[9] A great deal of attention has been focused on processes controlling the TTL water vapor budget and the H_2O concentration of air entering the stratosphere (H_2O_{entry}). Several studies have shown that cirrus formed in situ within the TTL can freeze dry air ascending through the cold tropopause region, reproducing observed water vapor concentrations, including interannual variability [e.g., *Gettelman et al.*, 2002; *Jensen and Pfister*, 2004; *Fueglistaler and Haynes*, 2005]. Both vertical and horizontal transport are important in determining H_2O_{entry}; horizontal transport in the TTL is very rapid while vertical transport is slow (it takes on the order of a few months for air parcels to ascend from 360 K to 390 K potential temperature; see Figure 2) [*Holton and Gettelman*, 2001]. To first order, the H_2O_{entry} will be controlled by the minimum temperatures encountered by air parcels in their journey upward through the TTL. This assertion is supported by the correspondence between a recent decrease in lower stratospheric humidity and the decrease in tropical tropopause temperatures [*Randel et al.*, 2004]. However, as discussed below, TTL cirrus clouds do not necessarily remove all vapor in excess of saturation, and details of the cloud microphysical properties and interactions with water vapor are important for understanding the dehydration process.

[10] The role of deep convection in the upper troposphere/lower stratosphere (TTL) water vapor budget is less well understood than the role of cirrus in removing water. Deep convection is certainly a source of water vapor and ice clouds to the TTL, and it is well established that extreme convective events can overshoot well into the stratosphere, resulting in local hydration events [*Liu and Zipser*, 2005, 2009; *Corti et al.*, 2008]. It also appears likely that convective injection

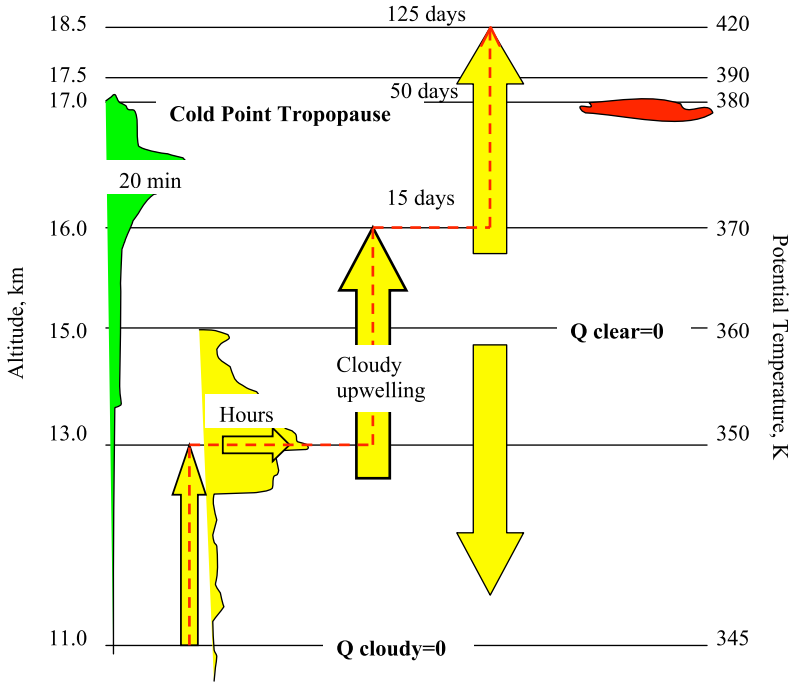

Figure 2. Schematic of three ideas to explain troposphere-to-stratosphere transport pathways across the TTL. Shown in green is an overshooting cumulus tower. The time for transport from the ground to just above the tropopause might be 20 min in such a tower; therefore, quite short-lived chemical species could enter the tropical stratosphere. During the 1980s it was argued that these convective penetrations would dehydrate the stratosphere. However, current data suggest instead that these penetrations are rare and hydrate the stratosphere. Once satellite data showed that the typical height for anvil detrainment is well below the tropopause, slower transport pathways were considered. In yellow, cumulus towers primarily detrain near 13 km. The red dashed line shows the path of air to the stratosphere in the model of *Corti et al.* [2006]. Slow uplift driven by radiative heating in cirrus lofts the air to about 16 km, where radiative heating in clear air propels the air across the tropopause, all of which may require about 2 months to go from the ground to the tropopause. Clear air below 16 km radiatively cools and sinks (yellow arrow without a red dashed line). In this model the average properties of clear air below the tropopause will be typical of air entering the stratosphere. The red subvisible cirrus indicates a third idea. In this case, air follows a path similar to the one in yellow until it reaches the tropopause. However, in this case the horizontal motions of air below the tropopause cause dehydration when the air mass is advected into colder than average regions of the TTL. The air is finally lofted across the tropopause in the last dehydration event due to radiative heating of subvisible cirrus. In this case the air in subvisible cirrus will be typical of that entering the stratosphere.

of ice into the often ice-supersaturated TTL can result in dehydration events [*Jensen et al.*, 2007]. Modeling studies have shown that convective injection throughout the TTL is required to explain observed concentrations of water vapor isotopes [*Dessler et al.*, 2007]. However, the overall impact of convection on water vapor abundance in the TTL remains poorly quantified.

[11] Figure 2 presents three visions of transport from the troposphere into the lower stratosphere. On the left side of Figure 2 the green cumulus has a turret overshooting the cold point tropopause. In this model, which has dominated thinking since the 1980s, air moves from the ground to the stratosphere in tens of minutes. The overshooting turret leaves dehydrated air behind in the stratosphere because the ice in the turret falls out too fast to evaporate in the stratosphere. It now appears that such over shooting convection does occur, but is rare in the tropics, and that such clouds generally hydrate the air, and only dehydrate if the air surrounding the turret is already supersaturated [*Liu and Zipser*, 2005; *Corti et al.*, 2008, *Jensen et al.*, 2007] The yellow cumulus clouds in Figure 2 represent the ideas of *Corti et al.* [2006]. These clouds detrain between about 12 and 15 km, with the most likely location being around 13 km, about a kilometer above the ceiling of the NASA DC-8. Air can reach these levels from the boundary layer in tens of minutes given the large vertical velocities in convective cores. The air detrains from the cores, and the anvil cloud can spread for several hours. If the ice in the anvil evaporates or falls out of the air parcel, the air parcel will radiatively cool and begin to descend. *Corti et al.* [2006] found that this descent is rapid. On the other hand, air parcels that retain ice will be radiatively heated and ascend. In about two weeks the parcels may have ascended to high enough altitudes to reach about 16 km, where clear-sky radiative heating can slowly drive them across the tropopause. The third view in Figure 2 is represented by the red subvisible cirrus. In models suggested by

Jensen et al. [1996], *Hartmann et al.* [2001] and *Holton and Gettelman* [2001] among others, it is assumed that convection hydrates the air below the tropopause. However, whenever the air moves horizontally into cold regions, cirrus clouds will form and dehydrate the air. The last step in this process occurs when air near the tropopause cools either due to vertically propagating waves, or due to horizontal transport into cold regions. Then subvisible cirrus form in situ, dehydrating the air mass, and vertical motions driven by radiative heating in the subvisible cirrus transport the dehydrated air into the stratosphere.

2.3. Tropical Clouds

[12] TC4 sought to improve understanding of the processes controlling the cirrus anvil production and evolution. These processes include the dynamics of the convection and the outflow anvil, cloud microphysics (droplet activation, ice crystal nucleation, coalescence, precipitation, etc.), and interactions between dynamics, microphysics, and radiation. These case study modeling efforts will serve both to improve the detailed cloud models and to provide insights for development of GCM cloud parameterizations.

[13] There have been several previous studies in the tropics related to deep convection. For instance, the 1974 Global Atmospheric Research Program Atlantic Tropical Experiment (GATE), the 1992–1993 Tropical Ocean-Global Atmosphere Coupled-Ocean Atmosphere Response Experiment (TOGA-COARE), and the 1993 Central Equatorial Pacific Experiment (CEPEX) all investigated the role of convection in the tropical energy budget. The 1987 Stratospheric Troposphere Exchange Project (STEP), on the other hand, investigated the role of convection in transporting water vapor into the stratosphere. TC4 brought new instruments to bear on some of these issues, but also had different goals. For example, TC4 measured the properties of tropical marine anvils in detail, which was not done in the previous tropical missions, but was done in tropical continental anvils in a TC4 predecessor mission the 2002 Cirrus Regional Study of Tropical Anvils and Cirrus Layers–Florida Area Cirrus Experiment (CRYSTAL-FACE) (*Jensen* et al. [2004]). TC4 also investigated the role of subvisible cirrus in exchange between the stratosphere and troposphere, as did its predecessor mission, the 2006 Costa Rica–Aura Validation Experiment CR-AVE. STEP, CRYSTAL-FACE and CR-AVE are outlined at http://www.espo.nasa.gov/missions.php.

[14] Anvil properties can be impacted by the aerosols which form nuclei to activate the water droplets at the base of clouds, heterogeneous nuclei which may lead to freezing inside clouds, or heterogeneous nuclei which may lead to particle formation in the anvils, or in other types of cirrus. Data collected in CRYSTAL-FACE indicated a connection between the anvil properties and the aerosols in the boundary layer and in the free troposphere [e.g., *Fridlind et al.*, 2004; *DeMott et al.*, 2003].

[15] TC4 planned to improve understanding of cirrus anvil evolution processes. The coverage of cirrus in the tropics depends on anvil lifetimes and the conversion of anvil outflow into self-maintaining cirrus layers. *Luo and Rossow* [2004] and *Mace et al.* [2006] show that a substantial portion of tropical cirrus is not directly associated with deep convection. While it is known that solar and infrared radiative heating in cirrus anvils can drive thermal instability and small-scale convection within the anvils, it is not known to what extent other factors such as a high background humidity or large-scale vertical motion contribute to tropical cirrus longevity. Factors likely to affect cirrus longevity include upper tropospheric humidity, large-scale dynamics, and wind shear, which in turn may be driven by radiative forcing impacted by cirrus. Extremely strong convective systems can generate cirrus with tops in the highest few kilometers of the troposphere. The final stage of these very high cirrus is unclear. As the larger ice crystals fall out, leaving behind optically thin cirrus, the clouds may be lofted by radiative heating, resulting in persistent thin cirrus as often observed near the tropopause.

[16] Tropical cirrus clouds are also frequently observed in locations remote from deep convection, perhaps existing as remnants of convective storms or formed by other processes acting on the water vapor mainly derived from deep convection [*Pfister et al.*, 2001]. These thin tropopause layer clouds can be formed in situ due to adiabatic ascent associated with equatorial waves such as the Kelvin wave [*Boehm and Verlinde*, 2000]. In the few kilometers at and just below the tropopause, laminar, optically thin (often subvisible) cirrus clouds occur frequently.

[17] Thin cirrus in the TTL occurs with very high frequency and may play a central role in regulating the water vapor concentration of the stratosphere. TTL cirrus has been observed with a number of satellites, including SAGE II, HALOE, and HIRDLS. More recently, CALIPSO measurements are providing a wealth of information about optically thin TTL cirrus regional distribution, structure, and extinction. In situ observations of TTL cirrus are limited, primarily because high-altitude aircraft are required to sample them.

[18] An understanding of the detailed processes of TTL cirrus formation is necessary for quantitative prediction of their impact on the water vapor and radiation budgets. Recent in situ observations suggest large supersaturations can occur both within TTL cirrus and in clear regions near the cold tropical tropopause [*Gao et al.*, 2004; *Jensen et al.*, 2005; *Peter et al.*, 2006]. The existence of such large supersaturations (relative humidities with respect to ice (RHI) sometimes approaching 200%) defies theoretical expectations that ice crystals will nucleate at 160% RHI, preventing further increase in supersaturation, and that within TTL cirrus, ice crystal growth should rapidly deplete vapor in excess of saturation. However, these high-supersaturation measurements have been called into question because of persistent discrepancies in water vapor measurements made by different instruments [*Jensen et al.*, 2008; *Krämer et al.*, 2009].

[19] There are significant gaps in our understanding of how cirrus forms at very low temperatures. The conventional theory is that homogeneous freezing of aqueous aerosols dominates production of ice crystals in the upper troposphere. However, recent measurements of TTL cirrus ice concentrations, particle size distributions, and cloud extinctions are in conflict with theoretical expectations for cirrus formed via homogeneous freezing at low temperatures [*Jensen et al.*, 2009b].

2.4. TTL Thermal Budget

[20] As discussed above, under clear-sky conditions, the upper part of the TTL is radiatively heated. In balance with this heating, the air is slowly ascending into the stratosphere. The rate of vertical transport through the TTL and lower stratosphere has been estimated from observations of the water vapor "tape recorder" [*Mote et al.*, 1996; *Niwano et al.*, 2003; *Schoeberl et al.*, 2008], from observations of the CO_2 gradient in the TTL [*Park et al.*, 2007; *Schoeberl et al.*, 2008], and from radiative transfer calculations [*Rosenlof et al.*, 1997]. It has also been pointed out that the TTL radiative heating rate depends on the presence of lower clouds; when cold, optically thick anvil cirrus is present below the TTL, the TTL will experience radiative cooling [*Hartmann et al.*, 2001].

[21] Recently, it has been recognized that cirrus within the TTL play an important role in the thermal budget. Radiative transfer calculations have shown that thin cirrus in the TTL can experience radiative heating of a few K/d [*Jensen et al.*, 1996; *McFarquhar et al.*, 2000; *Comstock et al.*, 2002]. *Corti et al.* [2006] suggested that radiative heating in TTL cirrus accounts for a large fraction of the total radiative heating in the TTL, and that radiatively driven lofting of cirrus may account for much the vertical transport from the main convective outflow level below the TTL up to the tropopause (see Figure 2). Measurements of TTL cirrus radiative heating rates, along with the microphysical properties of the clouds would be very useful for constraining radiative transfer calculations of TTL cirrus impacts on TTL heating and vertical transport.

[22] The ultimate role of tropical cirrus in future climate change involves feedback effects. For example, anthropogenic greenhouse gases can increase the surface temperature, possibly resulting in increased frequency and intensity of convective storms. Increased convection intensity could alter tropical cirrus cloudiness, with corresponding effects on the Earth radiation budget and additional surface temperature changes. Hence, the net effect of increased greenhouse gas concentrations on surface temperature depends on the response of convection and cirrus to the changing environment. Of course, the frequency and intensity of convection are sensitive to other parameters than just surface temperature, such as convective available potential energy (CAPE) and water vapor abundance. Prediction of these feedback effects requires understanding of the full cirrus lifecycle from generation in deep convection to horizontal spreading and ultimate dissipation. Understanding the balance between remote and local dynamical response to intensifying deep convection is a key issue, i.e., whether the local induced subsidence field is enhanced with resulting less or shorter-lived cirrus.

[23] Tropical cirrus may also be changing in response to anthropogenic aerosols. Particles from industrial activity or biomass burning may affect ice nucleation in the convective updrafts, ultimately changing the numbers and sizes of cirrus ice crystals. Likewise particulate and gaseous emissions that produce particulates, from either aircraft or volcanic eruptions, could alter cirrus properties. These cirrus modifications would ultimately affect radiation budgets and climate. While we know little about the composition or origins of aerosols in the tropical upper troposphere, recent work suggests that tropical cirrus that can be traced to deep convection do show a sensitivity to their convective sources [*Mace et al.*, 2006]. Recent field programs have shown surprisingly large amounts of organics, as well as metal and carbonaceous particles in the upper troposphere.

2.5. Chemical Fates of Short-Lived Compounds Transported From the Tropical Boundary Layer Into the TTL

[24] Until recently, the chemical precursors of the stratospheric radicals and aerosol, with the notable exception of water vapor, were thought to be compounds with long tropospheric lifetimes. This greatly simplified defining the chemical boundary condition for the stratosphere because globally averaged surface measurements of these long-lived compounds could be used. For example, sulfur was thought to be carried mainly by carbonyl sulfide, nitrogen by N_2O, and halogens by the relatively long-lived halocarbons.

[25] It has become increasing clear, however, that short-lived compounds transported to the tropopause region of the tropics significantly alter the chemistry of the global stratosphere. The amount of OCS transported across the tropopause accounts for no more than half of the sulfur aerosol present in the lower and middle stratosphere [e.g., *Weisenstein et al.*, 1997]. The remainder may come from small volcanic eruptions venting into the lower stratosphere, or from tropospheric sulfate and sulfur gases that are transported across the tropical tropopause. Thus, our understanding of how the "background" sulfate aerosol layer is maintained is incomplete. Bromine monoxide concentrations in the lower stratosphere appear to reflect the input of very short-lived bromine containing organic, and perhaps inorganic, compounds [e.g., *Ko et al.*, 1997; *Pfeilsticker et al.*, 2000], possibly leading to a much larger role for catalytic loss of lower stratospheric ozone by halogens than is considered in most models [*Dvortsov et al.*, 1999]. Finally, the concentration of reactive nitrogen, NO_y, and ozone are nonzero at the tropical tropopause [*Strahan*, 1999]. Release of NO_x from NO_y carried across the tropopause will likely have important implications for the efficiency of ozone loss by halogen cycles in the lower stratosphere. The NO_y/O_3 ratio can provide an important test of the realism of transport models for both the lower stratosphere and upper troposphere provided the sources of both species are understood [e.g., *Murphy et al.*, 1993].

[26] Observations of short-lived sulfur, nitrogen, and halogen-containing compounds in the region of the tropical tropopause are sparse. Acquiring such measurements is essential to accurately assess the effect on ozone of future changes in halogen loading, stratospheric sulfate aerosol abundance, and changes in tropical convection that might be associated with climate change. Estimates of the ozone depletion potential of short-lived halogen species depend on a quantitative evaluation of the efficiency of transport from source regions into the TTL and subsequent transport across the tropical tropopause. An understanding of the relative roles of (slow) large-scale transport and rapid convective transport and a better understanding of the chemistry of short-lived species in the UT and TTL is crucial to the improvement of such estimates [*Ko and Poulet*, 2002]. The observations of short-lived species in TC4 will address these issues and will

provide new understanding of dynamics in the UT and TTL regions. The interesting species for measurement have a range of photochemical lifetimes (e.g., 0.003 days for CH_2I_2; 4 to 7 days for CH_3I; 36 days for $CHBr_3$), and thus can be used to diagnose transport characteristics of the TTL on a variety of spatial and temporal scales.

2.6. Mechanisms That Control Ozone Below and Within the TTL

[27] Ozone concentrations in the TTL are determined by a complicated interplay of convective processes (that transport both ozone and short-lived compounds that fuel further ozone production from the lower troposphere), in situ photochemistry, and large-scale dynamics. Diagnosing this diversity of processes, occurring over large spatial and time scales, provides a challenging, but important, observational problem. To date, very few observations are available to test our understanding of the mechanisms that control ozone in the TTL.

[28] Photochemistry within the TTL is thought to lead to significant in situ ozone production. This production results primarily from the oxidation of CO by OH in the presence of nitrogen oxides. Ozone formation due to photolysis of molecular oxygen can also be important, because the stratospheric ozone column is relatively low in the tropics. Since the chemical lifetime of ozone with respect to photochemical loss is long (several months), the TTL is a region of significant net production for tropospheric ozone.

[29] Our current understanding of tropical tropospheric ozone in general is based primarily on insights drawn from analyses of data from aircraft campaigns and ozonesondes, and on model studies. In the upper tropical troposphere ($z > 12$ km), analysis of the few profiles obtained by the NASA ER-2, have demonstrated that HO_x photochemistry and its impact on ozone in this region is poorly understood [*McKeen et al.*, 1997; *Folkins et al.*, 1997; *Jaeglé et al.*, 1997; *Wennberg et al.*, 1998]. HO_x concentrations are much larger than expected based on H_2O/O_3 photochemistry. The high levels of HO_x observed, along with high NO_x, possibly associated with biomass burning, suggest elevated ozone production. Below 12 km (restricted by the flight altitude of the DC-8), major campaigns have taken place in the south tropical Atlantic (TRACE-A), or in the Pacific, flying out of Hawaii, Fiji, and Tahiti (PEM-Tropics A and B). Analyses of data from these campaigns have shown the importance of ozone precursor emissions from biomass burning in the dry season, and have also invoked an important role for lightning as source of NO_x upwind of the region of the measurements [*Thompson et al.*, 1996; *Jenkins et al.* 1997; *Schultz et al.*, 1999; *Staudt et al.*, 2002, 2003]. Over both the Pacific and South Atlantic photochemical reactions provide a net source for ozone above about 7 km and a net sink below, a consequence of the rapid decrease in water vapor with height. Over the tropical Pacific, production balances only about half of the column ozone loss below 12 km, indicating that there is significant transport of ozone to the Pacific [e.g., *Schultz et al.*, 1999; *Wang et al.*, 2001].

[30] As is clear from the above discussion, convection plays a key role in influencing the distribution of tropical ozone, both in terms of mixing ozone and its precursors out of the boundary layer over continental source regions (e.g., regions of biomass burning), and in mixing extremely low ozone values from either the marine boundary layer over the Pacific or unpolluted continental areas into the upper troposphere, as shown by analyses of ozonesonde data [*Kley et al.*, 1996; *Oltmans et al.*, 2001]. Lightning associated with convective systems will also provide a source of NO_x, enhancing photochemical ozone production.

[31] Analyses of ozonesonde profiles from Samoa have shown that ozone mixing ratios usually start to increase in the TTL around 14 km, well below the tropical tropopause [*Folkins et al.* 1999], although the largest change in gradient in the ozone mixing ratio is near the thermal tropopause. (The thermal tropopause is the World Meteorological Organization defined tropopause based on the lapse rate, which is generally lower in altitude than the cold point tropopause.) *Folkins et al.* [1999] argue that the increase in ozone is caused by the suppression of vertical mixing associated with convection above 14 km, and that the positive correlation they find between potential temperature and ozone above 14 km is consistent with slow large-scale ascent, positive radiative heating, and photochemical production of ozone. They also argue that some of the ozone originates from the stratosphere, based on correlations with N_2O.

[32] Increases in ozone well below the thermal tropopause are found at tropical ozonesonde sites in the Pacific, the Atlantic, and Africa. Inspection of individual profiles shows that this is not always the case, particularly in the western Pacific [*Takashima and Shiotani*, 2007]. The significant longitudinal gradients in tropical ozone, with values over the Atlantic higher than those over the Pacific year round, extend all the way to the thermal tropopause [*Logan*, 1999; *Thompson et al.*, 2003a].

[33] Long-lived tracers in TC4 should provide the foundation for diagnosing the processes that are responsible for atmospheric transport on the largest time and space scales (Figure 2). They should also provide a bridge tying together the objectives for the mission in midtropospheric chemistry, input processes to the stratosphere in the TTL, black carbon sources and distributions, and convective cloudiness and transport of water vapor.

[34] The land has very large exchange fluxes of CO_2 between the surface and the atmosphere. The signals from these fluxes appear above the stable marine planetary boundary layer (PBL), maintaining distinctive gradients between the marine PBL and the midtroposphere such as observed in CRYSTAL-FACE, providing a unique tracer for convective redistribution. The effect of the seasonal cycle of CO_2 on its vertical profile also offers an excellent age-of-air tracer for the TTL [*Park et al.*, 2007].

[35] Concentrations of SF_6 and/or HCFCs are growing rapidly in the atmosphere due to industrial sources predominantly in the northern hemisphere. These gases display distinctive north/south gradients and thus provide good indicators of the hemisphere of origin for air in the study domain. They also represent independent age-of-air tracers, albeit usually less sensitive than the CO_2 seasonal cycle.

2.7. Linking Satellite and Aircraft Data

[36] Resolution of many of the issues discussed above will require remote sensing measurements from satellite instruments with near global spatial coverage and multiyear temporal coverage. For example, understanding how cirrus

Table 2. TC4 Science Flights

Date	DC-8	ER-2	WB-57	Comments
13 July	X			Transit to Costa Rica
14 July		X		Transit to Costa Rica
17 July	X	X		
19 July		X		DC-8 not flown due to flap actuator problem
21 July	X			ER-2 not flown (some instruments down)
22 July	X	X		
24 July	X	X		Lightning strike on DC-8
25 July		X		DC-8 not flown due to lightning strike on DC-8 on previous flight
28 July	X			ER-2 not flown (some instruments down)
29 July	X	X		
31 July	X	X		
3 August	X	X	X	Transit to Costa Rica, WB-57F
5 August	X	X	X	
6 August	X	X	X	
8 August	X	X	X	
9 August		X	X	Return home
10 August	X			Return home
13 August			X	Houston WB-57F science flight

clouds impact regional and global upper tropospheric humidity clearly requires analysis of large-scale fields of cloudiness and H_2O abundance. Remote sensing constituted an important part of the TC4 measurement campaign by providing the horizontal distributions of cloud properties and gas concentrations at a variety of spatial and temporal scales. Cirrus cloud properties also vary on small spatial scales, and in situ observations of ice crystal size distributions, total condensed water, and extinction will be critical for validating algorithms applied to remote sensing measurements.

[37] There are numerous examples of field programs involving aircraft and balloon platforms that have successfully linked with satellite validation ranging back over at least 2 decades. The SOLVE-2 program was aimed at validating SAGE III, which obtained profiles of aerosols, ozone, and a number of other chemical species at high latitudes. Measurements obtained during SOLVE-1/THESEO-2000 provided validation of chemical ozone loss rates, O_3 and H_2O profiles, and polar stratospheric cloud detection and analyses (e.g., denitrification inferred from PSC formation temperature) from the Naval Research Laboratory Polar Ozone and Aerosol Monitor (POAM) III satellite instrument [*Newman et al.*, 2002]. Aircraft measurements of CO from the DC-8 during TRACE-P provided validation of MOPITT data on Terra [*Jacob et al.*, 2003]. Satellite remote sensing was a central theme of CRYSTAL-FACE [*Jensen et al.*, 2004]. CRYSTAL-FACE provided validation opportunities for Terra, Aqua and TRMM. Not only were cloud property retrieval algorithms tested, but specific case studies were proposed by the satellite groups and carried out. Some of these involved clear-sky data as well as cloudy data. The TC4 field campaign supported validation efforts of the entire "A train": Aura, CALIPSO, CloudSat, PARASOL and Aqua. It also provided validation opportunities for Terra and TRMM.

[38] The Aura satellite, a principal focus of TC4, provides essential information on the spatial and temporal variability of key constituents in the TTL region (such as ozone, water vapor, CO, and thin cirrus clouds) with horizontal and vertical resolutions not previously available from satellite observations. Satellite observations in this region are, however, generally more challenging than measurements at higher altitudes due to the cloud cover.

3. Mission Scope

[39] Complex field programs require a significant amount of preparation, which is often not acknowledged. The NASA Earth Science Project Office (ESPO) began preparations for TC4 in September 2006. A large amount of work was performed on the hangars, lab/office modifications, and obtaining all the lab and aircraft ground support equipment required for the mission. International agreements for the aircraft overflight and personnel country clearances were also arranged with all the various countries.

[40] Over 70 instruments were integrated onto the three aircraft based at different locations. The DC-8 was integrated at McClellan Field in California, the ER-2 at NASA's Dryden Flight Research Center in California, and the WB-57F at NASA's Ellington Field in Houston, Texas. ESPO provided coordination and support at each of these integration sites and managed the C-5 military airlifts to transport all the aircraft and investigator equipment to and from the mission deployment site.

[41] In Las Tables, Panama, preparations were made for the NPOL radar and NATIVE atmospheric research trailer. The ground site required a road to be built, the hill leveled, and electricity to be brought to the site. Because of the remoteness of the site, communications were obtained through a portable KU satellite ground.

3.1. Location and Timing

[42] The TC4 aircraft were based at the Juan Santamaria International Airport in Alajuela, a suburb of San Jose, Costa Rica (10.0°N, 84.22°W) (Figure 1). The first data flights were made on 17 July 2007 and the last data flight from Costa Rica was made on 8 August 2007 (Table 2). The WB57-f made one additional data flight from Houston, Texas, on 13 August 2007. The final date of the field mission was chosen to minimize the chance of tropical storms or hurricanes, which become more likely in September. The initial dates of the field mission were chosen to maximize the chance that the intertropical convergence zone (ITCZ) with its extensive convective activity, would be near Costa Rica.

[43] In addition to the aircraft, balloons and a Doppler radar (the Shared Mobile Atmospheric Research and Teaching Radar, SMART-R) were positioned at the Juan Santamaria airport.

[44] A polarization radar (NPOL), a ground station (NATIVE), and further balloon launches were conducted from Las Tablas, Panama. This location was chosen because of its proximity to the Gulf of Panama. It was expected that convection would form frequently in the Gulf and that the aircraft would be able to fly into the anvils of these clouds guided by the radar. While such flights did occur, the convection over the Gulf of Panama was often very intense, and low wind shear kept the anvils near the convective updrafts. These conditions made it difficult to safely operate the aircraft over the Gulf of Panama.

Table 3. Satellite Instruments

Instrument	Satellite	Investigator	Institution	Measurements of Relevance to TC4	Cross-Track Swath Width
OMI	Aura	P. Levelt	KNMI	SO_2, aerosols	2600 km
TES	Aura	R. Beer	JPL	Ozone	5 km
HIRDLS	Aura	J. Gille	NCAR	Temperature profiles	300 km
MLS	Aura	N. Livesey	JPL	Cloud and water vapor	300 km
CALIOP	CALIPSO	D. M. Winker	NASA Langley	Aerosol extinction	100 m
Cloud Profiling Radar	CloudSat	G. Stephens	Colorado State, JPL	Radar backscatter	1.4 km
MODIS	Terra	V. Salomonson	NASA Goddard	Cloud properties	2330 km
MODIS	Aqua	V. Salomonson	NASA Goddard	Cloud properties	2330 km
Precipitation radar, Microwave imager	TRMM	S. Braun	NASA Goddard	Rainfall rates	215 km
Visible and infrared imager	GOES 10/12	P. Minnis	NASA Langley	Cloud properties	Hemispheric

[45] Balloon launches were also conducted from San Cristobal a SHADOZ site [*Thompson et al.*, 2003b] in the Galapagos Islands. This has been a water vapor measurement site since 1998 [*Vömel et al.*, 2002].

3.2. Platforms

[46] Here we discuss the numerous platforms used in TC4 including satellites, aircraft, balloons and ground-based facilities.

3.2.1. Satellites

[47] A number of satellites were employed. AURA has four instruments designed to measure air chemistry (Table 3). Operational considerations required that the ER-2 and WB-57F land before the midafternoon overflight times of AURA. However, the DC-8 was able to make a large number of flights under various Aura instruments. Since the AURA instruments have variable fields of view, it generally was only possible to be directly in the field of view of a single instrument during the satellite overpass. Many of the DC-8 flights were aimed at the OMI instrument, and determining if SO_2 emissions from South American volcanoes were properly evaluated.

[48] The MODIS instruments on the Terra and Aqua satellites routinely retrieve cloud properties from all types of tropospheric clouds. Because of the wide observing area, it was often possible to underfly the Terra satellite during its morning overpass. Hence the TC4 aircraft were able to investigate such retrieved parameters as cloud top and base heights, cloud particle size and cloud ice water content. The DC-8 was also able to underfly Aqua along with the rest of the A-Train satellites.

[49] CloudSat and CALIPSO, along with Aura, are part of the A-Train constellation of satellites which all pass a given spot on Earth within a few minutes of each other. CloudSat obtains radar backscatter data, while the CALIOP instrument on CALIPSO uses a lidar to sense optically thin clouds. Numerous DC-8 flights had segments dedicated to underflying these instruments. For instance, flights were made to investigate the properties of marine boundary layer clouds to help interpret the satellite observations near the surface. The ER-2 and DC-8 cloud and precipitation radars also profiled a number of cloud systems for comparison with the data from these satellites.

[50] The instruments on the TRMM satellite are aimed at measuring precipitation and its vertical structure. Underflights for comparison with the ER-2 and DC-8 radars were made.

3.2.2. Aircraft

[51] Three NASA aircraft were employed in TC4.

[52] The NASA ER-2 is the civilian version of the second generation Lockheed U-2 high-altitude aircraft. The ER-2 has flown in numerous field campaigns. It is capable of flights

Figure 3. The NASA ER-2 and its instrument complement as flown in TC4.

Table 4. ER-2 Instruments

Instrument	Name	Primary Investigator	Products
CPL	Cloud Physics Lidar (532, 1064 nm)	Matthew McGill, NASA GSFC	Cloud/aerosol detection and layer information (top/base altitudes, extinction)
CRS	Cloud Radar System (94 GHz)	Gerry Heymsfield, NASA GSFC	Radar reflectivity, Doppler velocities, cloud layer water content
EDOP	ER-2 Doppler Radar (X band)	Gerry Heymsfield, NASA GSFC	Radar reflectivity, Doppler velocities, precipitation
AMPR	Advanced Microwave Precipitation Radiometer (10.7, 19.4, 37, 89 GHz	Robbie Hood, NASA MSFC	Precipitation Index
MAS/MASTER	MODIS, MODIS-ASTER (starting July 29) Airborne Simulator (VIS/NIR/SWIR/IR spectrometer)	Michael King, NASA GSFC	Cloud properties, ice and water (cloud top, optical thickness, effective particle size, WP)
CoSSIR	Conical Scanning Sub-mm Wave Imaging Radiometer (183–874 GHz)	James Wang, NASA GSFC	IWP, ice cloud median mass particle diameter, moisture profiles
S-HIS	Scanning High Resolution Interferometer Sounder (3–18 μm)	Hank Revercomb, Univ. Wisconsin	Temperature/moisture profiles, cirrus cloud properties (top pressure, optical thickness, effective particle size), IWP
BB IR	Broad Band Radiometer (4–42 μm)	Anthony Bucholtz, NRL	IR radiative fluxes and layer heating rate (with similar instrument on DC-8)
SSFR	Solar Spectral Flux Radiometer (VIS-SWIR)	Peter Pilewskie, U. Colorado	Solar spectral fluxes and layer heating rate (also on DC-8), ice cloud properties
MTP	Microwave Temperature Profiler	M.J. Mahoney, NASA JPL	Temperature versus pressure altitude near aircraft, molecular number density versus pressure altitude
MVIS	Video Camera	Jeff Myers, Ames	

above 20 km (pressures less than 50 hPa) for durations up to 8 h. The ER-2 flew 13 science flights in TC4 including the transit flights (Table 2).

[53] The ER-2 aircraft was used as a remote sensing platform. Its basic goal was to simulate various satellite instruments so that more prolonged comparisons of in situ and remote sensing data could be made than would be possible between satellites and aircraft. Figure 3 illustrates the ER-2 with the locations of the 11 instruments. Table 4 lists the ER-2 instruments, their PI, and provides a brief summary of their measurement capabilities. Video from the ER-2 camera is available at ftp://asapdata.arc.nasa.gov/outgoing/MVIS/TC4/.

[54] The NASA WB-57F has been flying research missions since the 1960s when it was originally used for sampling the atmosphere for the debris from nuclear weapons tests. The aircraft is capable of flights to 60,000 ft (19.4 km) for durations approaching 6.5 h. Prior to the start of TC4 the WB-57F suffered a fire in its landing gear that damaged panels on the wing. It was, therefore, delayed in arriving at Costa Rica. The WB-57F flew six science flights in TC4 including two ferry flights, and one local science flight from Houston, Texas.

[55] The WB-57F was used as an in situ sampling aircraft in TC4. One of its major goals was to underfly the ER-2 and measure cloud properties as seen by the ER-2 remote sensing instrument. It was also well instrumented with in situ instruments for sampling tracers of air motion, and trace gases. Figure 4 illustrates the WB-57F with the locations of the 25 instruments. Tables 5a and 5b list the WB-57F instruments, their PIs, and their measurement capabilities.

[56] The NASA DC-8, managed during TC4 by the University of North Dakota, is a former commercial airliner that has been converted into a flying laboratory. The DC-8 has been deployed in numerous field campaigns. The aircraft is capable of flights to an altitude of 12 km for durations over 10 h. It made 13 science flights during TC4 including the transit flights (Table 2).

[57] The DC-8 was used in TC4 both to remotely sample the atmosphere and to make in situ measurements of aerosols, clouds and gases. While numerous flight segments were flown in anvils, a number of flight segments were also flown to investigate emissions from volcanoes and from the jungles of Central and South America. The aircraft is shown in Figure 5, with the locations of the 25 instruments. The DC-8 instruments are listed in Table 6 along with the PI, and an overview of the measurements.

3.2.3. Balloon Sondes and Ground-Based Stations

[58] A total of 214 Vaisala RS92-SGP radiosondes were released at Juan Santamaria International Airport between 16 June and 15 August by the Ticosonde-TC4 project. Launches were made twice daily at 0000 and 1200 UT through 30 June and four times daily at 0000, 0600, 1200 and 1800 UT thereafter. As outlined in Table 7 the sondes provided pressure, temperature, relative humidity and GPS winds every 2 s up to a campaign-average altitude of 30.1 km.

[59] The Ticosonde-TC4 project was led by Henry Selkirk of the BAER Institute of Sonoma, California and NASA-Ames Research Center, in collaboration with Walter Fernandez and Jorge Andrés Diaz of the Escuela de Fisica at the Universidad de Costa Rica (UCR), Jorge Amador of the Centro de Investigaciones Fisicas at UCR, Werner Stolz of the Instituto Meteorologico Nacional (IMN) and Pedro León of the Centro Nacional de Alta Tecnologia (CeNAT). Launches

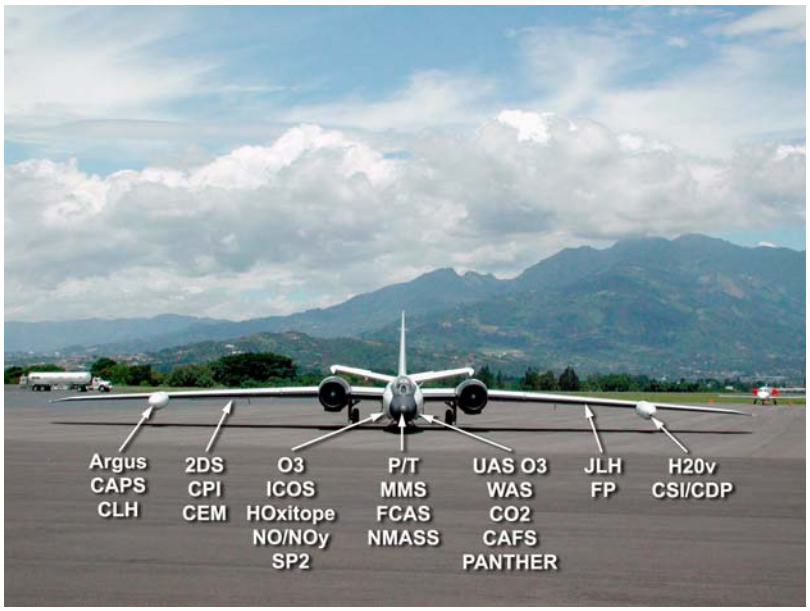

Figure 4. The NASA WB-57F and its instrument complement as flown in TC4.

were conducted by IMN personnel in collaboration with UCR students at the IMN sonde site at the west end of the airport.

[60] A team led by Holger Vömel of the University of Colorado (CU) and the NOAA Earth Systems Research Laboratory (ESRL) (now at Deutscher Wetterdienst, Meteorological Observatory Lindenberg) made 15 launches of balloons carrying the CU Cryogenic Frostpoint Hygrometer (CFH) [*Vömel et al.*, 2007a] and the ECC ozonesonde [*Komhyr et al.*, 1995] from the IMN sonde site. The CFH-ozonesonde launch program was a partnership with IMN and Jessica Valverde of the Universidad Nacional (UNA) and IMN. The CFH-ozonesonde launches were made approximately every other day during the aircraft flight campaign by a team composed of IMN staff and students from UNA. The typical altitude achieved by the 1200-g CU balloons was 30 km. Vömel also cooperated with the Instituto Nacional de Meteorología y Hidrologia of Ecuador to conduct a simultaneous CFH-ozonesonde launch program at San Cristobal, Galapagos.

[61] A team led by Sergei Khaykin of the Central Aerological Observatory in Dolgoprudny, Russia flew their Lyman-α FLASH-B (FLuorescent Advanced Stratospheric Hygrometer) hygrometer [*Vömel et al.*, 2007b] along with the CFH on five nighttime ascents.

[62] Launches of both radiosondes and the water vapor sondes and ozonesondes were coordinated with ozonesonde launches at Las Tablas, Panama, by a team led by Anne M. Thompson of the Penn State University and Gary Morris of Valparaiso University.

Table 5a. WB-57F in Situ Water and Particle Instruments

Instrument	Name	Primary Investigator	Products
CLH	Closed-Path Laser Hygrometer	Linnea Avallone, U. Colorado	Ice water content
Frostpoint (FP)	Frostpoint Hygrometer	David W. Fahey, NOAA	Water vapor mixing ratio
H2Ov	Water Vapor	Elliot Weinstock, Harvard	Water vapor mixing ratio
HOxotope	HOx/Isotope	Tom Hanisco Harvard	Total water (vapor + condensed), H_2O and HDO
ICOS	Integrated Cavity Spectrometer	Tom Hanisco, Harvard	Water vapor isotopologue ($H_2^{16}O$, $H_2^{17}O$, $H_2^{18}O$, HDO) and CH_4 mixing ratio
JLH	JPL Laser Hygrometer	Robert Herman, NASA JPL	H_2O mixing ratio
2DS	2D-S Probe	Paul Lawson, SPEC Inc.	Cloud particles images, particle size distributions
CAPS	Cloud, Aerosol and Precipitation Spectrometer	Bruce Gandrud, Droplet Measurements	Concentration, ice water content, surface area, extinction coefficient
CDP	Cloud Droplet Probe	Bruce Gandrud, Droplet Measurements	Concentration, ice water content, surface area, extinction coefficient, median volume diameter
CEM	Transmissometer	Paul Lawson, SPEC Inc.	Cloud extinction
CPI	Cloud Particle Imager	Bruce Gandrud, Droplet Measurements	Cloud particles images, particle size distributions, particle concentration, cloud extinction, ice water content
CSI	Cloud Spectrometer Impactor	Paul Lawson, SPEC Inc.	Condensed (ice plus liquid) water content
FCAS	Focused Cavity Aerosol Spectrometer	J. C. Wilson, Denver University	Number of particles/mg air in 28 size bins from ~90 to ~1300 nm
NMASS	Nuclei Mode Aerosol Size Spectrometer	J. C. Wilson, Denver University	Number of particles/mg air larger than 4 nm, 8 nm, 16 nm, 32 nm, 50 nm
SP2	Single Particle Soot Photometer	Ru-Shan Gao, NOAA	Black carbon

Table 5b. WB-57F Trace Gas, Atmospheric State, and Remote Sensing Instruments

Instrument	Name	Primary Investigator	Products
Argus	Diode Laser Spectrometer	Max Loewenstein, NASA Ames	CO, CH_4, N_2O
NO/NO_y	Nitric Oxide/ NOy Chemiluminescence	Andy Weinheimer, NCAR	NO and NO_y, NO, NO_2, NO_y
O3	Ozone	David W. Fahey, NOAA	O_3 mixing ratio
PANTHER	Gas Chromatograph	James W. Elkins, NOAA	PAN, CO, H_2, Methane, N_2O, SF_6, CFC-11, CFC-12, CFC replacement compounds (HCFC-22, -141b,-142b) and hydrofluorocarbons, (HFC-134a), halon 1211, methyl halides (methyl chloride (CH_3Cl), methyl bromide, (CH_3Br), methyl iodide (CH_3I), carbon disulfide (CS_2) and carbon sulfide (COS).
CO_2	Harvard CO_2	Bruce Daube, Harvard University	CO_2
UAS O3	Ozone	Ru-Shan Gao, NOAA	O_3 mixing ratio
WAS	Whole Air Sampler	Elliot Atlas, University of Miami	Numerous trace gases
MMS	Pressure Transducer and Temperature Probe	Paul Bui, NASA ARC	Pressure, temperature, 3D winds
P/T	Pressure and Temperature	David W. Fahey, NOAA	Pressure, temperature
CAFS	Actinic Flux Spectrometer	Rick Shetter, NCAR	Actinic flux
ACAM	Digital Camera	Scott Janz, NASA GSFC	Forward scene

[63] Two radars were used in TC4. Michael Biggerstaff from the University of Oklahoma led the first international deployment of the Shared Mobile Atmospheric Research and Teaching Radar (SMART-R) during the NASA TC4 experiment. The radar was located near the west end of the Juan Santamaria International Airport in Costa Rica (Figure 6), where it was used to provide real-time flight support for NASA's DC-8, ER-2, and WB-57 aircraft. The SMART radar was the first Doppler radar to ever have been deployed in Costa Rica and provided insight into the structure and timing of the modified land-sea breeze circulation that initiates afternoon thunderstorms over the airport on a regular basis.

[64] The NASA Polarimetric (NPOL) research radar is a state-of-the-art weather research radar. It was based near the Gulf of Panama at Las Tablas, Panama (see Figure 7). The goal of this radar was to observe deep convective systems developing in the Gulf of Panama, and to safely guide research aircraft into the anvils of cumulonimbus.

[65] The Nittany Atmospheric Trailer and Integrated Validation Experiment (NATIVE) is a self-contained, state of the art, mobile research facility designed for satellite validation, air quality monitoring, investigations of pollution transport and deposition, and for use as an educational outreach tool (see Figure 7). The facility houses a suite of in situ trace gas instruments, active and passive remote sensing instruments for atmospheric profile and column measurements, and several meteorological probes. The satellite communication system allows NATIVE to disseminate results in near real time.

4. Mission Forecasting and Aircraft Coordination

[66] While forecasts were important in setting up the flight profiles, in practice the aircraft were guided to interesting

Figure 5. The NASA DC-8 showing the instruments used in TC4 and their placement on the aircraft.

Table 6. DC-8 Instruments

Instrument	Name	Primary Investigator	Products
DLH	Open Path TDL	Glen Diskin, NASA LaRC	H_2O
2D-S, CPI	Cloud Probes	Paul Lawson, SPEC Inc.	Cloud particle size distribution and type (habit)
LARGE	Aerosol Spectrometers	Bruce Anderson, NASA LaRC	Particle size distribution, optical properties, CCN
PALMS	Particle Composition Mass Spectrometer	Dan Murphy, NOAA	Particle composition
CAPS, PIP	Cloud Probes	Andy Heymsfield, NCAR	Cloud particle size, images
CVI	Counterflow Virtual Impactor	Cynthia Twohy, Oregon State	Cloud water content
CIMS	Chemical Ion Mass Spectrometer	John Crounse, Caltech	Acids and organic peroxides, SO_2
DACOM	TDL (DACOM)	Glen Diskin, NASA LaRC	CO, CH_4, N_2O
FAST OZ	Chemiluminescence Ozone Probe	Melody Avery, NASA LaRC	Ozone mixing ratio
MACDON-NA	IR gas analyzer	Stephanie Vay, NASA LaRC	CO_2
SAGA	Mist Chamber	Jack Dibb, U. New Hampshire	NO_3^-, SO_4^-, aerosol composition
NO	Chemiluminescence Nitric Oxide	Ron Cohen, U. C., Berkley	NO
TD-LIF	Tunable Diode Laser	Ron Cohen, U. C., Berkley	NO_2, Alkylnitrates, PAN
WAS	Whole Air Sampler	Don Blake, U. C., Irvine	Many trace gases
Dropsondes	Atmospheric Probe	Errol Korn, NCAR	Temperature, pressure, winds, relative humidity
MMS	Pressure and Temperature Probe	Paul Bui, NASA ARC	Pressure, temperature, winds
APR-2	Precipitation Radar	Eric Smith, NASA MSFC	Reflectivity, precipitation
LASE	IR Lidar	Ed Browell, NASA LaRC	Water vapor, aerosol and cloud heights, aerosol type
DIAL	UV Lidar	Ed Browell, NASA LaRC	Ozone, aerosol and cloud heights, aerosol type
BB IR	Broadband Radiometer	Anthony Bucholtz NRL	IR radiative fluxes and layer heating rate
CAFS	UV-Vis Actinic Flux	Rick Shetter, NCAR	Ozone zenith column
SSFR	Solar Spectral Flux Radiometer	Peter Pilewskie, U. Colorado	Solar spectral fluxes and heating rate
DC-8 CAM	Video	Rick Shetter, U. N. Dakota	Nadir and forward video

phenomena in real time. We describe both of these activities below.

4.1. Forecasting

[67] Mission forecasting was led by Lenny Pfister and Henry Selkirk in conjunction with local forecasters from Costa Rica. Some of the forecasting tools available are discussed by *Pfister et al.* [2010]. Two aspects of the mission depended on the forecasting group.

[68] Daily forecasts were used to determine the locations of promising meteorological targets. Such targets were highly varied because of the extensive payloads. For example, the cores and anvils of mesoscale complexes were interesting targets to achieve cloud related objectives. Subvisible cirrus, and the lower stratosphere were targeted to understand cross tropopause transport. Plumes of dust from the Sahara were interesting to understand aerosol properties and removal processes. South American volcanoes and jungles were of interest for satellite validation and air chemistry studies. The aircraft configurations varied for these different objectives. For instance, in sampling anvils and subvisible cirrus, we stacked the aircraft so that vertical profiles could be obtained and so that the data sensed remotely by the ER-2 could be measured in situ by the other aircraft. We also attempted to sample the same cloud regions with the WB-57F and the DC-8 to compare sensors on one occasion. We frequently used the DC-8 alone after the other aircraft finished their missions, due to its longer duration than the other aircraft, for satellite under flights, and explorations of volcanoes and jungles in South America.

[69] The second goal of forecasters was to determine if adverse weather might prevent safe mission operations. Fortunately no tropical storms occurred during TC4, and no missions were canceled due to weather. However, intense afternoon convection at the Juan Santamaria airport was almost a daily occurrence. On several occasions commercial

Table 7. Ground-Based Instruments and Balloons

Instrument	Primary Investigator	Period of Operation	Location	Products
Ticosonde	Henry Selkirk, Bay Area Environmental Research Institute	16 June through 15 August 2007	Juan Santamaria International Airport	Geopotential height, pressure, temperature, relative humidity, GPS winds, latitude and longitude at 0.5 Hz
CFH-ozonesondes	Holger Vömel, University of Colorado	1 July through 12 August 2007	San Cristobal, Galapagos/ Juan Santamaria Airport	Ozone and water vapor plus temperature, pressure and GPS winds at ~1.4 Hz
NATIVE	Anne Thompson, Pennsylvania State University		Las Tablas, Panama	Temperature versus pressure, ozone, water vapor, winds
SMART	Michael Biggerstaff, University of Oklahoma		Juan Santamaria airport	Weather radar
NPOL	John Gerlach, NASA Goddard Space Flight Center		Las Tablas, Panama	Polarization radar
NATIVE	Anne Thompson, Pennsylvania State University		Las Tablas, Panama	Ozone, NO/NO_y, SO_2, CO, lidar, Sun photometer, UV radiometer Aerosol size distribution

Figure 6. The University of Oklahoma SMART radar located at Juan Santamaria International Airport in Costa Rica.

airliners had to be diverted, experienced long weather delays, or landed in heavy rainfall with lightning in the area. None of these conditions were desirable for landing, particularly for the ER-2 and WB-57F. Aside from aircraft safety, heavy rain could damage instruments before the aircraft could be put into their hangars.

[70] As a consequence of the severe afternoon weather we relied heavily on the Costa Rican forecasters to predict the time of onset of convection. Generally, we planned to land the ER-2 and WB-57F between 1200 and 1400 local time to avoid convection. We also monitored the local convection while the aircraft were in flight. The skill of the forecasters was a critical element in not having to divert any aircraft, and in generally being able to hangar the aircraft before tropical downpours began.

4.2. Real-Time Flight Plan Coordination

[71] There are a number of reasons to control research aircraft in real time. When sampling the anvils of mesoscale convective complexes, safety requires that the aircraft stay away from the convective cores, or at least sample cores that have weak updrafts, or are decaying. In addition, given real time knowledge of the locations of interesting atmospheric phenomena, nearly instantaneous aircraft control allows one to change opportunistic sampling into controlled investigations. During the CRYSTAL-FACE mission in July 2002 in southern Florida, we were able to use the large number of meteorological radars in Florida together with the U.S. air traffic control reporting information, which is based on aircraft transponders, to navigate as many as 5 aircraft in real time. In contrast, Costa Rica has no weather radars, even at its main airport, and does not provide tracking information on aircraft.

[72] NASA installed Research Environment for Vehicle-Embedded Analysis on Linux (REVEAL) systems on a number of aircraft including the DC-8, ER-2 and WB-57F. TC4 was the first opportunity to employ REVEAL on all of these aircraft simultaneously. REVEAL, developed and supported the NASA Dryden Flight Research Center, allows aircraft location, and instrument data to be reported back to mission operations. It also allows for scientists on the ground to communicate back to the NASA DC-8 flight scientist to discuss changes in flight plans. The DC-8 pilots in turn could communicate these changes to the WB-57F and the ER-2. However, we also had ground communications with these aircraft through a "ground-based" ER-2 pilot. In conjunction with REVEAL, the Real Time Mission Monitor (RTMM), developed and supported by the NASA Marshall Space Flight Center, allowed us to locate the aircraft on a virtual Earth display, track their motions in the context of meteorological data, and to down-link data from the aircraft that could be used to alter the aircraft flight plans in real time. For example, the mission operations group was able to see in near real time the aircraft locations, several satellite data sets on clouds, data on recent lightning strikes, and data from our own aircraft including lidar profiles of clouds. Using tools developed by Patrick Minnis and his group at NASA Langley (P. Minnis et al., Cloud properties determined from

Figure 7. The NASA polarization (NPOL) radar and the NATIVE trailer located in Las Tablas, Panama.

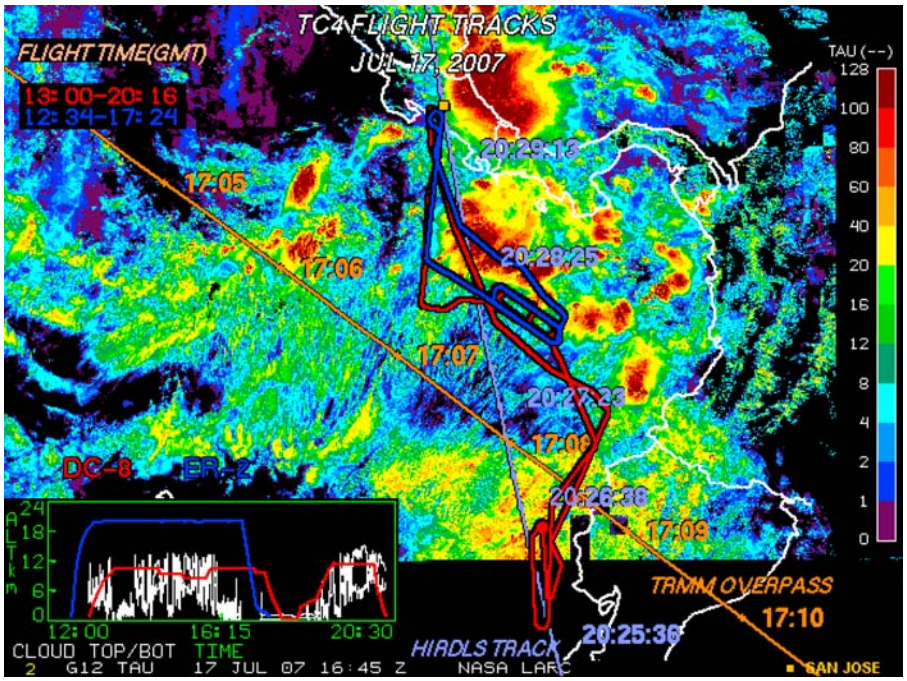

Figure 8. The ER-2 (blue) and DC-8 (red) flight tracks for 17 July 2007 are superimposed on a GOES retrieved optical depth map. Approximate takeoff and landing times are given for the DC-8 and ER-2 in the top left corner. San Jose, Costa Rica (10.0°N, 84.22°W), is marked with a yellow square. The aircraft altitudes are given in the bottom left insert. The flight tracks are superimposed on cloud optical depth retrieved from the GOES image, whose time is given in the black bar at the bottom. Note that optical depths above 100 are reported in the core of the mesoscale complex, while most of the aircraft sampling was in regions with optical depths in the range from 1 to 10. The locations and times of a TRMM overpass and a HIRDLS overpass are also shown. Note that the swath width for satellite sensors is highly variable; see Table 3. Base image is available at http://www-angler.larc.nasa.gov/tc4/flttrks/jul17/products/ALL_ALL.TAU.2007198.1645.gif.

GOES and MODIS data during TC4, submitted to *Journal of Geophysical Research*, 2010) we were also able to combine the aircraft location data with Geostationary Operational Environmental Satellite (GOES) Rapid Scan data to aid in detecting fresh convective cells embedded in the mesoscale clusters we were studying. Finally, we had real time data from the NPOL and SMART radars to help locate the aircraft relative to convection in flights near the Gulf of Panama, or on return to the Juan Santamaria airport in Costa Rica.

[73] As discussed below, many of our flight plans involved coordinated flights for several aircraft early in a mission, and then different flight plans at the end of the mission. These flight plans were partly the result of the short flight duration of the WB-57F relative to the other aircraft. However, they also reflected the strong diurnal cycle of convection at the Juan Santamaria airport. Generally the ER-2 and WB-57 had landing times in the period from noon to 2pm local to avoid bad weather on landing. However, the DC-8 is less sensitive to weather conditions on landing than the other aircraft. The DC-8 often returned in the late afternoon, commonly in heavy rainfall.

[74] Animated overlays of the flight tracks and various satellite observed and derived cloud parameters can be found at http://www-angler.larc.nasa.gov/tc4/flttrks. Animated overlays of observed quantities including lightning strikes can be found at http://rtmm.nsstc.nasa.gov/movies-TC4.html. There was an unprecedented level of aircraft coordination in TC4. On multiple flights, we had hours of anvil cirrus sampling with the in situ and remote aircraft in a stacked formation. These data should be very useful for evaluation of the remote sensing retrievals, and for others interested in vertical structures in anvils. Examples will be discussed below.

5. Aircraft Flights

[75] Table 2 outlines the aircraft flights made during TC4. Flight plans and flight reports are available at http://www.espo.nasa.gov/TC4/flightDocs.php. We will discuss the flights individually below.

5.1. Flight on 17 July 2007

[76] Figure 8 illustrates the flight tracks for the ER-2 and DC-8 on 17 July 2007. The aircraft linked up south of a large mesoscale complex off the Pacific coast of Costa Rica. The aircraft then did several oval loops, or racetracks, with the DC-8 sampling cirrus anvils from the cloud system, and the ER-2 remotely observing the cloud field from above. The ER-2 then returned to San Jose flying over the cores of several convective cells during a TRMM overpass. The DC-8 flew along the coast of Ecuador to sample the

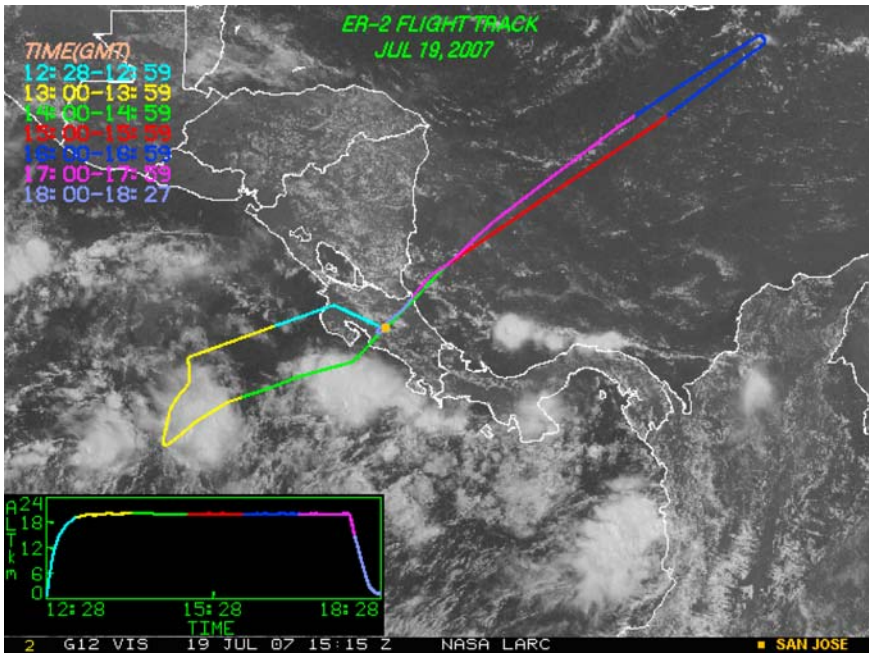

Figure 9. The ER-2 flight track for 19 July 2007. Labels are explained in Figure 8. The flight track is superimposed on a visible image which composites GOES 10 and GOES 12 data. Base image is available at http://www-angler.larc.nasa.gov/tc4/flttrks/jul19/ER2.SEG.GOESVIS.2007200.1515.gif.

emissions from volcanoes, and then flew along a HIRDLS track for the Aura satellite before returning to Costa Rica. In Figure 8 the flight tracks are superimposed on cloud optical depths retrieved from the GOES satellite data. Note that the three racetracks flown by the aircraft are in low optical depth cirrus rather than in the high optical depth portion of the cloud north of the racetrack. The southern region of the image is black, because that marks the southern boundary of the GOES 12 observations.

5.2. Flight on 19 July 2007

[77] Figure 9 illustrates the flight track for the ER-2 on 19 July 2007. The DC-8 did not fly due to a mechanical problem. The ER-2 first flew over the Pacific to profile the cores of several convective systems. It then flew over the Caribbean where it detected low-lying layers of Saharan dust, whose presence had been predicted. The aircraft also observed a high altitude, optically thin cirrus cloud as it returned to Costa Rica.

5.3. Flight on 21 July 2007

[78] Figure 10 illustrates the DC-8 flight track on 21 July 2007 superimposed on a GOES 10 + 12 composite visible image. The ER-2 had a mechanical problem on this day and did not fly. The flight began with a low-level run to sample the marine boundary layer over the Pacific, and then sampled cirrus in the convective regions over the Gulf of Panama. The DC-8 then proceeded to Colombia to sample the plume of the volcano Nevado de Huila, which shows up on OMI SO_2 imagery. The DC-8 then turned north to obtain a trace-gas sample of the Colombian farming regions, which may be a source of methane. Finally the DC-8 sampled Saharan dust aerosols in the Caribbean, of the sort sampled by the ER-2 on 19 July, and returned to Costa Rica.

5.4. Flight on 22 July 2007

[79] Shortly after takeoff, the DC-8 headed southwest into the Pacific and descended into the boundary layer for aerosols and chemistry sampling as shown in Figure 11. An ITCZ convective system was sampled, and a box pattern was set up for sampling the outflow cirrus. The long sides of the rectangle were oriented approximately across the mean wind direction. This strategy allowed the DC-8 to sample many distinct outflows from individual convective cells, with the ER-2 directly overhead. The DC-8 vertically profiled several times through the outflow cirrus (in and out of cloud) between about 7.6 and 10.6 km in close coordination with the ER-2. When the outflow cirrus appeared to be dissipating, the DC-8 did several penetrations through small, developing convective turrets at temperatures ranging from 200 to 255 K before heading west to Panama to sample cirrus generated by Gulf of Panama convection earlier in the day. The along-wind track took the DC-8 through two separate anvil outflows that were streaming southwestward from dissipating convective sources. The DC-8 did two legs, coordinated with ER-2 profiling enroute through the cirrus between about 7.6 and 11.6 km. Crystals as large as 3 mm and ice water contents as large as 0.3 g/m^3 were detected over the Gulf of Panama. The ER-2 departed for Costa Rica, while the DC-8 headed north along the CloudSat/CALIPSO track, flying through optically thin cirrus at about 12 to 12.5 km which existed above a mostly cloud free ocean surface. This cirrus contained pristine ice crystals (bullet rosettes were noted on the CPI). CloudSat and CALIPSO passed overhead as the DC-8 approached its most northerly point on the several hundred kilometer leg. At that point, the DC-8 turned back south along the satellite track and, after an Air Traffic Control delay, spiraled down into the boundary layer to

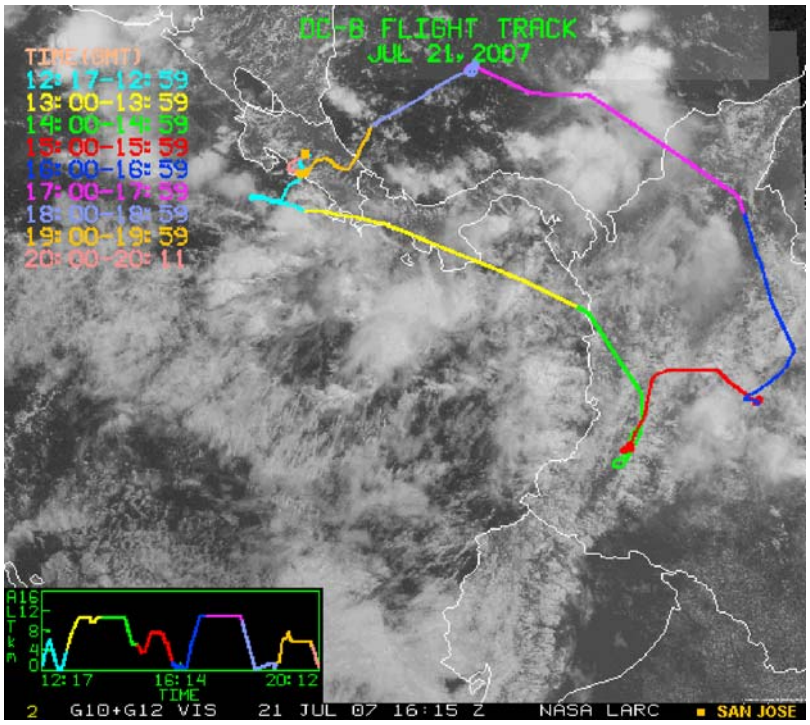

Figure 10. The DC-8 flight track for 21 Jul, 2007. The flight track is on top of a visible wavelength GOES image. Labels are explained in Figure 8. Base image is available at http://angler.larc.nasa.gov/tc4/flttrks/jul21/DC8.ALL.GOESVIS.2007202.1615.gif.

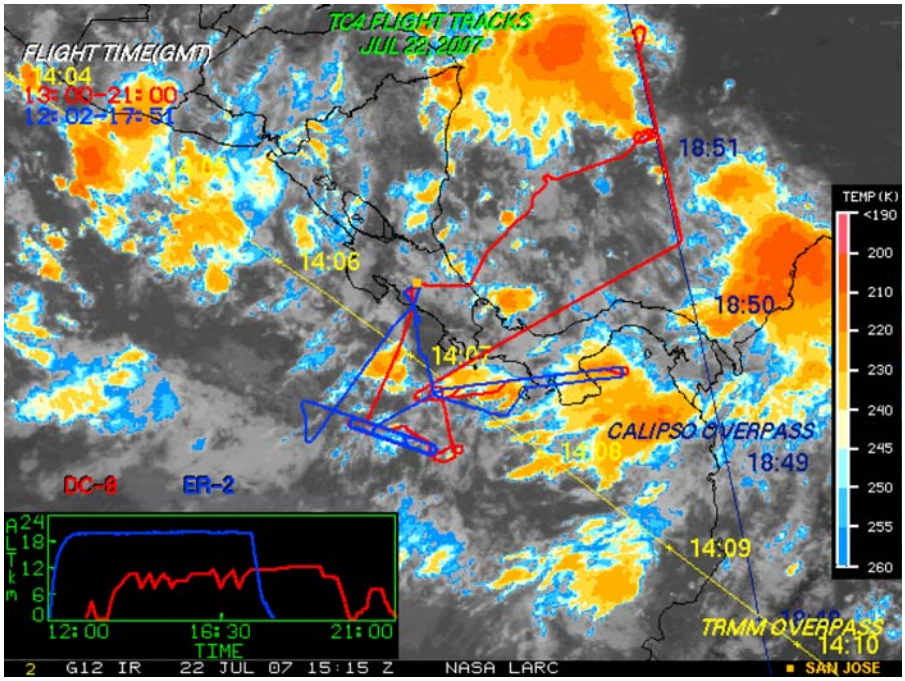

Figure 11. The ER-2 and DC-8 flight tracks for 22 July 2007. Figure labels are explained in Figure 8. Also noted are overpass paths for TRMM (yellow) and CALIPSO (blue). The background is a GOES 10+Goes 12 infrared brightness temperature image. Base image is available at http://www-angler.larc.nasa.gov/tc4/flttrks/jul22/ALL_ALL.GOESIR.2007203.1515.gif.

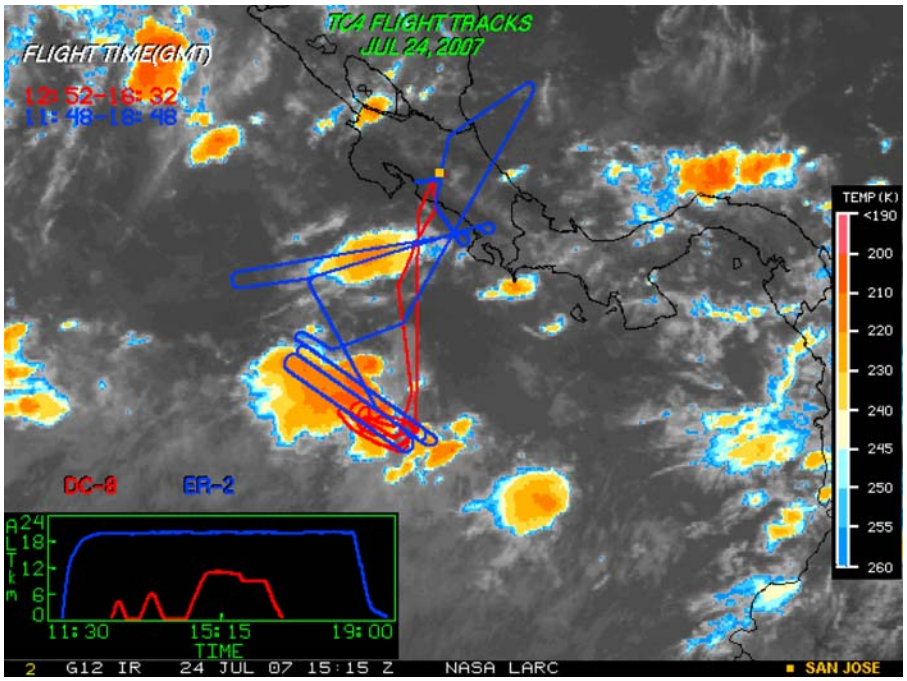

Figure 12. The tracks of the DC-8 and ER-2 for 24 July 2007. For an explanation of the keys, see Figure 8. The flight tracks are superimposed on a GOES infrared brightness temperature image. Base image is available at http://www-angler.larc.nasa.gov/tc4/flttrks/jul24/ALL_ALL.GOESIR.2007205.1528.gif.

sample Saharan dust below 4 km indicated by the DC-8 lidars. After stepping up to about 2 and 3 km, the DC-8 returned to base. Over the entire flight profiles of aerosols, tracers, and chemical species were collected from the boundary layer to the upper troposphere both in the Pacific and Caribbean, and a variety of types of anvil outflow cirrus were sampled in situ.

5.5. Flight on 24 July 2007

[80] As shown in Figure 12, the DC-8 first did a low-level run through the boundary layer around a convective system. It then ascended to near 20,000 feet where the plane was struck by lightning twice in a rapidly developing system. The DC-8 then did the boundary layer run again and ascended to 36 kft to probe the cirrus layer. The aircraft was in and out of anvils at 30 kft, then ascended to 36 kft (this part of the flight was fairly rough); apparently the aircraft penetrated the core. At this point the flight was terminated to inspect the aircraft for damage due to the lightning strike.

[81] The ER-2 initially flew northeast over the Caribbean into relatively clear air while gaining altitude. The ER-2 then flew southwest along a line with relatively clear air below the aircraft in order to profile aerosol concentrations with its lidar. On this leg, a layer of cirrus was observed in a 12 to 15 km layer. In addition, there was a layer of aerosol extending from the surface to 3 km in the Caribbean. After reaching the southwestern point over the Pacific at about 1320 UT, the ER-2 flew two racetrack patterns in a counterclockwise pattern in coordination with the DC-8 before shifting to a second track for a third rounding. After the DC-8 encountered a lightning strike, the ER-2 was shifted northward to a track that was over a convective core that had a considerable cirrus shield. The ER-2 flew approximately three legs over this core and returned to Costa Rica.

5.6. Flight on 25 July 2007

[82] Figure 13 illustrates the ER-2 flight track on 25 July 2007. The DC-8 did not fly because damage from the lightning strike on 24 July was being assessed. Low tropopause temperatures were forecast along the coast of Nicaragua, and the goal for the flight was to measure the radiation budget in subvisible cirrus. The ER-2 detected a subvisible cirrus in the low albedo area off the eastern coast of Nicaragua in Figure 13, where GOES did not detect any cloud optical depth. After an initial pass above the cloud, the ER-2 slowly descended through the cloud to make the first measurements of the heating rate in subvisible cirrus. The heating rate is critical to determine if subvisible cirrus pump freeze-dried air into the stratosphere. The ER-2 also profiled Saharan dust crossing from the Caribbean into the Pacific using the lidar.

5.7. Flight on 28 July 2007

[83] Figure 14 illustrates the flight path of the DC-8 on 28 July 2007. The ER-2 did not fly due to instrument repair issues. The goal of the DC-8 flight was to profile the Saharan dust layer, and to gain further information about dust removal as air crosses Central America. The DC-8 first flew over the Caribbean and identified the dust with lidar, it then descended to sample the dust in situ. A similar flight profile was then flown in the Pacific.

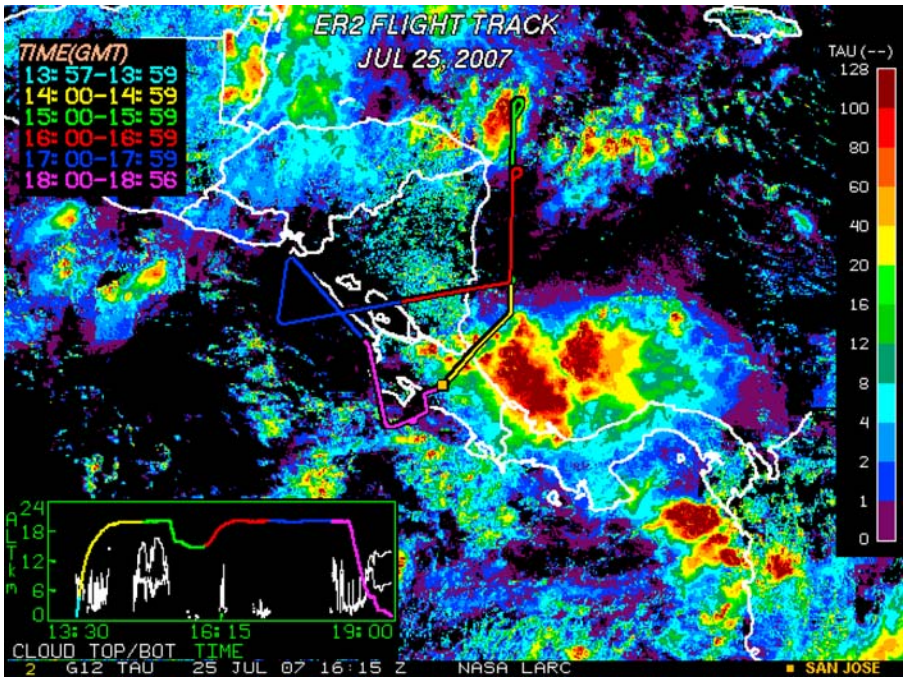

Figure 13. The track of the ER-2 for 25 July 2007. For an explanation of the keys, see Figure 8. The GOES image has been processed to obtain the cloud optical depths. Base image is available at http://www-angler.larc.nasa.gov/tc4/flttrks/jul25/products/ER2.TAU.2007206.1615.gif.

5.8. Flight on 29 July 2007

[84] Figure 15 illustrates the flight tracks for the ER-2 and DC-8 on 29 July 2007. The goal of these flights was to investigate the microphysical properties of the marine stratus layers off the coast of South America, in order to help CloudSat and CALIPSO better interpret their observations of these clouds. The ER-2 and DC-2 coordinated a flight leg along the coast of South America and under the TERRA

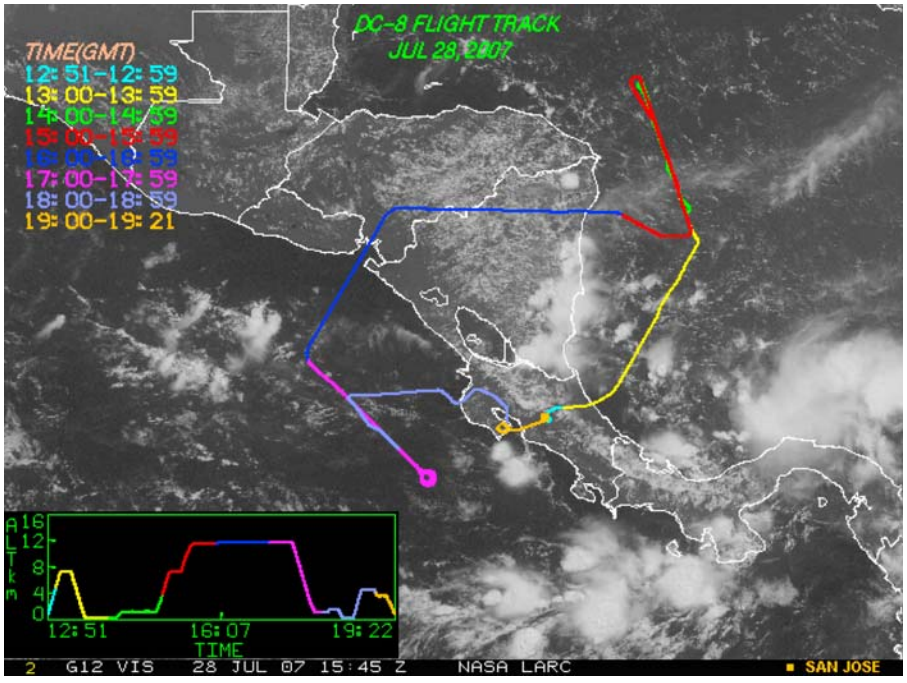

Figure 14. The DC-8 flight track for 28 July 2007 superimposed on a GOES visible image. For an explanation of the keys, see Figure 8. Base image is available at http://angler.larc.nasa.gov/tc4/flttrks/jul28/dc8_index.html.

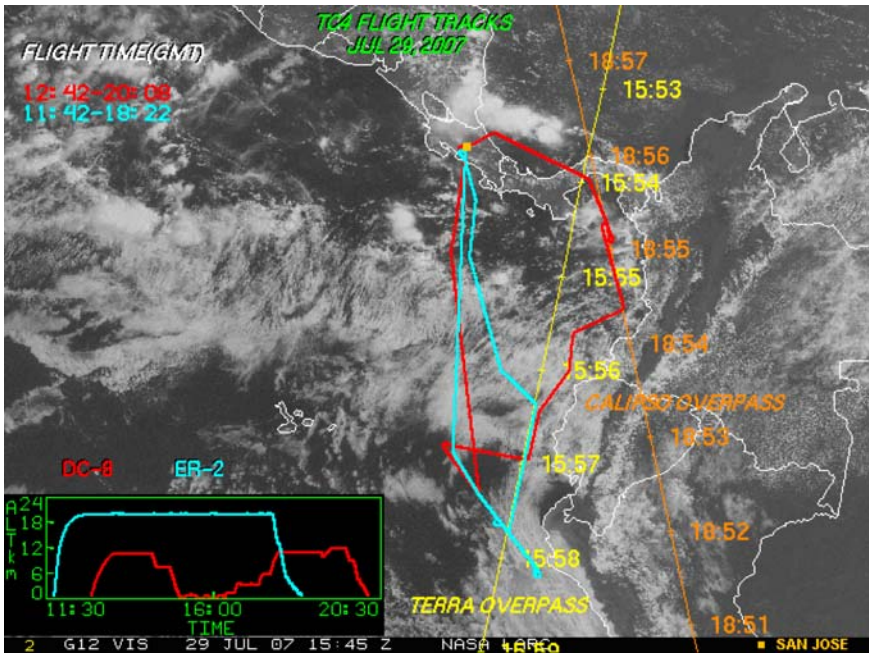

Figure 15. The DC-8 and ER-2 flight tracks for 29 July 2007 superimposed on a GOES 10/12 composite visible image. See Figure 8 for explanations of the other information given. Note that the yellow line is the TERRA overpass line, while the orange line is the CALIPSO/CloudSat track. Base image is available at http://angler.larc.nasa.gov/tc4/flttrks/jul29/allplane_index.html.

overpass, across stratus with varying structure. The ER-2 then returned to Costa Rica, while the DC-8 flew through a series of convective cells, one of which was encountered during the CloudSat and CALIPSO overpass. The DC-8 also sampled air in the Gulf of Panama within the radar beam from the Panama ground site.

5.9. Flight on 31 July 2007

[85] Figure 16 illustrates the aircraft flight paths for 31 July 2007 superimposed on a GOES retrieval of ice water path. The ER-2 and DC-8 first did a series of racetracks over southern Costa Rica. The goal was to sample the anvil from the large mesoscale complex in the Pacific just off the coast of Costa Rica. Figure 17 provides a view of this mesoscale complex from the DC-8. Following this anvil sampling the ER-2 flew over the convective cores in the complex, then returned to base. Meanwhile the DC-8 proceeded upwind of the complex and did a vertical profile to understand the properties of the materials entering the convection.

5.10. Flight on 3 August 2007

[86] Figure 18 illustrates the flight tracks of the DC-8, ER-2 and WB-57F on 3 August 2007 superimposed on a GOES infrared image. The DC-8 and ER-2 proceeded across Nicaragua, where they met the WB-57F near the border with Honduras. The three aircraft flew though a small convective system. After the WB-57F landed in Costa Rica, the ER-2 and DC-8 proceeded to the ground site in Panama, where they sampled the anvils from a convective complex. The DC-8 made a descent over the Panama ground site, while the ER-2 returned to Costa Rica. The DC-8 then sampled the remnants of a convective system over the Pacific, as it followed the CloudSat and CALIPSO overpass track back to Costa Rica.

5.11. Flight on 5 August 2007

[87] Figure 19 illustrates the flight tracks of the DC-8, ER-2 and WB-57F on 5 August 2007 superimposed on a GOES infrared image. The principal goal of this flight was to obtain a vertical profile of cloud properties in the anvil of a convective complex. The three aircraft did a stacked flight in the Pacific near the Gulf of Panama. The ER-2 flew over a convective core near the Panama ground site. After the departure of the other aircraft, the DC-8 did a spiral descent into the boundary layer over the ocean near Columbia to sample the inflowing air to the convective complex. It then flew over the Columbian jungles to sample the air there. Finally it flew over the Panama ground site on its return to Costa Rica.

5.12. Flight on 6 August 2007

[88] Figure 20 illustrates the flight tracks of the DC-8, ER-2 and WB-57F on 6 August 2007 superimposed on a GOES image. The principal goal of this flight was to explore the structure of the TTL as far south of Costa Rica as possible. Some of the flight occurred in subvisible clouds, which were sampled directly by the WB-57F and remotely by the ER-2 and DC-8. The DC-8 sampled the boundary layer near the Galapagos Islands, part of which included crossing through a Von Kármán vortex to the north of the Galapagos (Figure 21). The DC-8 returned to Costa Rica along a Terra overpass track.

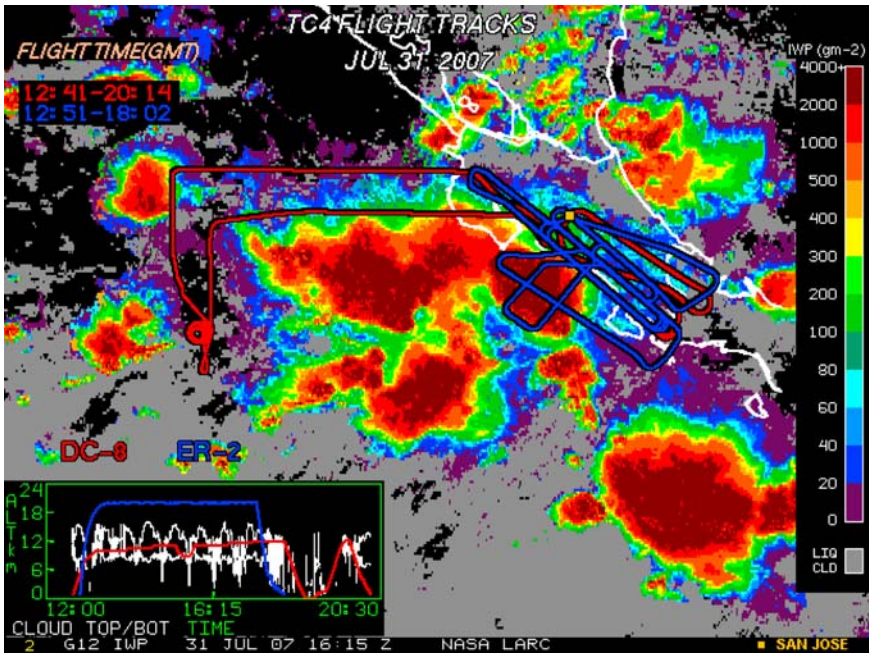

Figure 16. The flight tracks of the ER-2 and DC-8 on 31 July 2007 superimposed on a GOES retrieval of ice water path. For an explanation of the keys, see Figure 8. Base image is available at http://www-angler.larc.nasa.gov/tc4/flttrks/jul31/products/ALL_ALL.IWP.2007212.1615.gif.

5.13. Flight on 8 August 2007

[89] Figure 22 illustrates the flight tracks of the DC-8, ER-2 and WB-57F on 8 August 2007 superimposed on a GOES infrared image. The primary goal of this flight was to sample the anvil blowing downwind from a large mesoscale complex in the Pacific Ocean south of Costa Rica. As the anvils evolved the aircraft first made measurements roughly normal to the wind direction, and across the anvils. Later the aircraft were aligned with the wind direction and made measurements along the anvils in increasingly aged air. The WB-57 and DC-8 flew consecutive flight legs through the same anvil cirrus at altitudes of 11.4 and 12 km for comparison of microphysical measurements made on the two platforms. When the WB-57 departed for Costa Rica, the ER-2 flew to a newly developing set of cells and flew over several convective cores. After the return of the ER-2 and WB-57F to Costa Rica, the DC-8 made low-level observations over the rain forest in Columbia. The DC-8 then flew over the Panama ground site on its return to Costa Rica.

6. Progress Toward the TC4 Goals

[90] The papers in this special section, as well as papers using TC4 data published elsewhere, have helped address many of the TC4 goals. Much data also remains to be analyzed or applied.

6.1. Meteorological Setting

[91] An important set of questions for the meteorological context of TC4 that *Pfister et al.* [2010] address are: (1) what are the basic flow patterns in the region, and how typical are those patterns; (2) what is the character of the convection, and how does it compare to previous years; (3) what are the implications of convection and circulation for the origin of air masses sampled during the experiment; and (4) how does the convection and flow vary during the three week period of the experiment?

[92] In the TTL, the global circulation is dominated by the Asian Anticyclone, and the easterly winds that persist from the western Pacific to the Atlantic Ocean. *Pfister et al.* [2010] find that during TC4, easterly winds were stronger than normal; instead of a weak, fluctuating pattern between east-

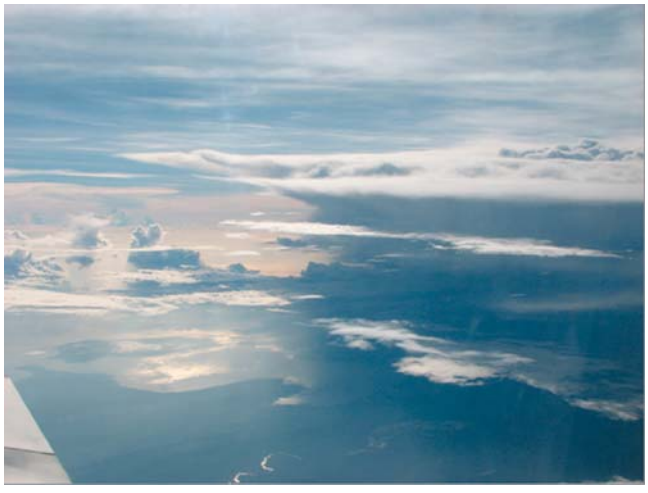

Figure 17. The convective complex seen from the DC-8 at the southern edge of the race tracks in Figure 16, where the sky was relatively clear. In most of the race track the DC-8 was flying relatively low in the anvil, where ice crystals were falling down from above. The ER-2 recorded the cloud tops near 15–16 km, well above the DC-8 ceiling of 12 km. Photo by Paul Wennberg.

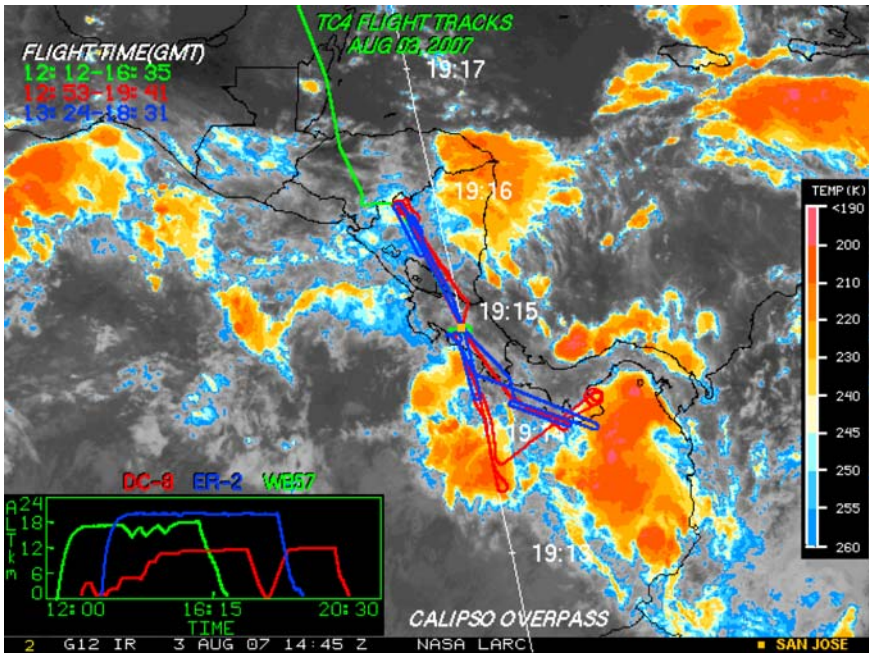

Figure 18. The DC-8, ER-2, and WB-57F flight tracks for 3 August 2007 superimposed on a GOES infrared brightness temperature image. The white line is the CloudSat and CALIPSO overpass track. For an explanation of the keys, see Figure 8. Base image is available at http://www-angler.larc.nasa.gov/tc4/flttrks/aug03/ALL_ALL.GOESIR.2007215.1428.gif.

erlies and westerlies over Central America, easterly winds dominated with only occasional interruptions. The August phase of the experiment, in particular, had strong easterlies in the TTL. In the upper troposphere, the character of the flow in the TC4 region is determined by the North American anticyclone, the mid-Atlantic trough and the Central American convective maximum. Though convective divergence was

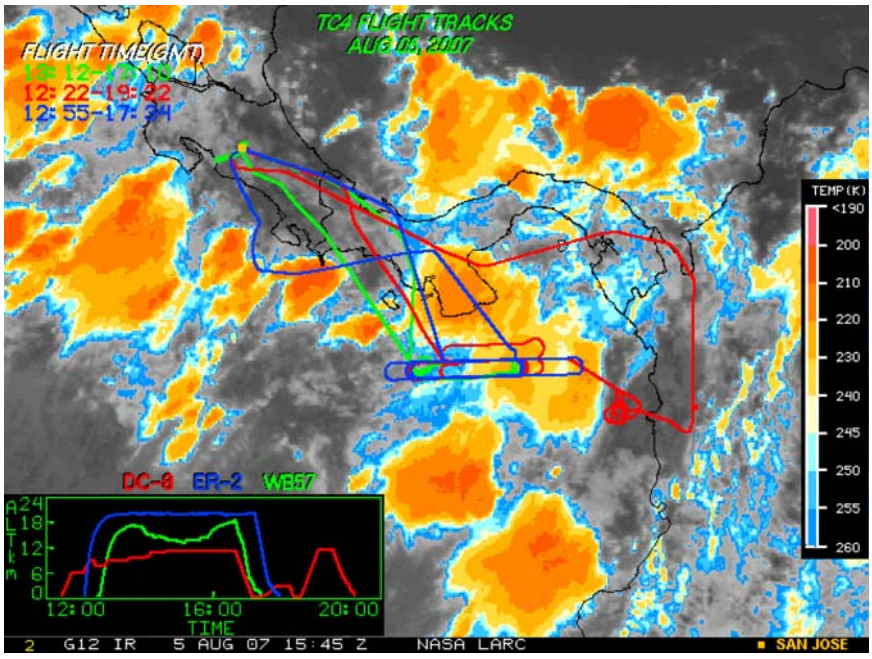

Figure 19. The flight tracks of the DC-8, ER-2, and WB-57F on 5 August 2007 superimposed on a GOES infrared brightness temperature image. For an explanation of the keys, see Figure 8. Base image is available at http://www-angler.larc.nasa.gov/tc4/flttrks/aug05/ALL_ALL.GOESIR.2007217.1558.gif.

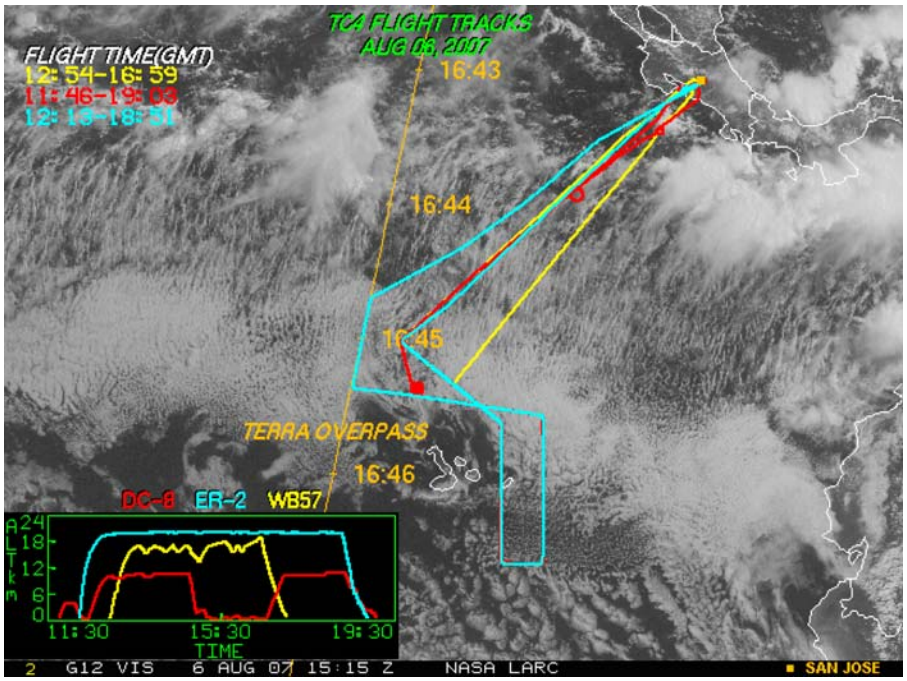

Figure 20. The flight tracks of the DC-8, the ER-2, and the WB-57F on 6 August 2007 superimposed on a GOES 10+12 visible image. The yellow line is the Terra overpass track. For an explanation of the keys, see Figure 8. Base image is available at http://angler.larc.nasa.gov/tc4/flttrks/aug06/allplane_index.html.

obviously less than normal, the basic flow was similar to previous years.

[93] *Pfister et al.* [2010] find that convection was significantly weaker than in previous years, with areas of coldest cloud top temperatures in the Gulf of Panama reduced by upward of 25% compared to more active years (like 2005). In fact, the incidence of cold cloud tops in the outgoing longwave radiation climatology was among the three lowest out of the 34 years sampled. The anomalously low incidence of cold cloud tops was most likely due to the ENSO cycle, specifically anomalously cold sea surface temperatures off the coast of South America.

[94] The flow patterns and convection determine the origin of the air. An important feature of air at low levels is the strong contribution from flow over the Sahara, reflected in observations of Sahara dust during TC4. *Pfister et al.* [2010] find that in the southern portion of the area surveyed by the aircraft, a significant amount of air originated from the Amazon region. In the upper troposphere, some air was transported from long distances at upper levels and was not directly influenced by convection in the immediate region. Convectively influenced air at 200 mbar came from Central America, the northern Amazon region, the Atlantic ITCZ, and the North American monsoon. Because of the basic easterly pattern, only a limited number of air parcels in the upper troposphere originated from convection in the eastern Pacific. In the TTL, the basic easterly flow pattern meant that convection to the east, including African and Asian convection, could affect the observed air masses. Near San Jose and northward, African and Asian convection (aged as much as 20 days) may have contributed as much to the air masses as Central and South American convection. South of 8°N, Asian and African convection had far less impact because the easterly flow is weaker.

[95] *Pfister et al.* [2010] find there was a strong diurnal cycle in the convection, with the frequency of deepest convection peaking over the oceans at night and in the morning hours. There was variation on longer time scales. The first 5 days of the experiment were relatively convectively active, with a strong easterly wave pattern. For the next 2 weeks, easterly waves were relatively weak, and convection was generally less intense. For the last 8 days, convection was strong, which coincided with a strong easterly wave pattern.

[96] Meteorological data were collected from balloons, satellites and the aircraft as discussed further below. J. Dean-Day et al. (An evaluation of MMS pressure, temperature and horizontal wind accuracy, submitted to *Journal of Atmospheric and Oceanic Technology*, 2010) examine the accuracy of the in situ meteorological measurements on the DC-8 and WB-57F.

6.2. Questions 1 and 2: What Controls Humidity in the Upper Troposphere and Lower Stratosphere?

[97] *Selkirk et al.* [2010] describe balloon sonde measurements of water vapor and ozone using the Cryogenic Frostpoint Hygrometer (CFH) and electrochemical concentration cell (ECC) ozonesondes at Juan Santamaria International Airport during TC4 as well as during the Tropical Convective Systems and Processes (TCSP) mission in July 2005. In addition, they discuss high-resolution radiosondes launched 4 times daily from mid-June through mid-August in both years. The CFH measurements show that the upper troposphere was frequently saturated in both campaigns, sometimes in layers with stratospheric levels of ozone and at other

Figure 21. A false color MODIS-Aster Airborne Simulator (MASTER) image of the Von Kármán vortex sampled by the DC-8 on August 6 2007 just north of the Galapagos Islands (RGB = 2.1, 1.6, and 0.66 μm channels). The light blue color indicates relatively large cloud droplet sizes in these stratus clouds. The instrument's swath width (vertical dimension) is about 37 km, while the length of the flight leg is about 90 km. Image courtesy of Steven Platnick.

times with low ozone indicative of uplifted tropospheric layers. They find dehydration near the cold point tropopause (CPT) in many profiles, and they attribute these cold events to equatorial waves forced by regional convection. While the waves are responsible for large temporal variability in cold point water vapor mixing and saturation mixing ratios as well as ozone mixing ratio in the upper troposphere and at the CPT, they find that dehydration of nascent stratospheric air occurred no higher than a kilometer above the mean level of the CPT which lay at 16.6 km and ~375 K.

[98] Time-height sections of radiosonde temperature and wind anomalies reveal coherent westward moving wave variations in the lower stratosphere extending down to the ~15 km level. *Selkirk et al.* [2010] find these waves produce temperature fluctuations on the order of ±7 K in the stratosphere and are the driver of water vapor variations and dehydration near the tropopause as well as variations of ozone due to vertical displacements across the strong mean gradient. In contrast to this wave-driven regime, below the 15 km level, which is approximately the neutral buoyancy level for deep convection, the waves rapidly weaken with height and water vapor variations become decoupled from temperature; in this region, the observed supersaturations that are observed are most likely closely associated with detrainment of deep convective clouds and anvils. Similarly, the weakening of wave displacements in this convective regime below 15 km yields a strong decrease in the relative variability of ozone, and vertical mixing is the dominant process causing ozone variability.

[99] An important issue with respect to water is the role of convection in establishing the water vapor mixing ratio. *Sayres et al.* [2010] report measurements from the ICOS and HOxotope water isotope instruments and Lyman-alpha hygrometer made during CR-AVE and TC4 to explore the role convection plays in setting the water vapor mixing ratio of the TTL and air entering the tropical stratosphere. Isotopologue ratios are heavy compared to the predicted value based on temperature as the sole control of the water vapor mixing ratio, but are consistent with convective ice lofting throughout the TTL. Using a convective influence model and a simple parameterized model of dehydration along back trajectories, *Sayres et al.* [2010] show that the predominant profile of isotopologue ratios can be explained by convective injection of isotopically heavy water vapor only into the lower part of the TTL. Such convective injection is consistent with the second and third mechanisms for water transport illustrated in Figure 2. However, the measurements clearly show examples of air parcels with significantly enhanced water vapor mixing ratios and isotopologue ratios as compared to the mean profiles both below and above the summertime tropical tropopause, though ice particles from convection at these altitudes were not directly observed during the flight campaigns. The convective influence model shows that these air parcels were mixed with convective outflow near the western tropical Pacific at altitudes lower than the observations, but still near the local tropical tropopause.

6.3. Question 3: What Are the Properties of Thin Cirrus and What Controls Them?

[100] Considerable progress was made in understanding the properties of subvisible cirrus. *Bucholtz et al.* [2010] describe

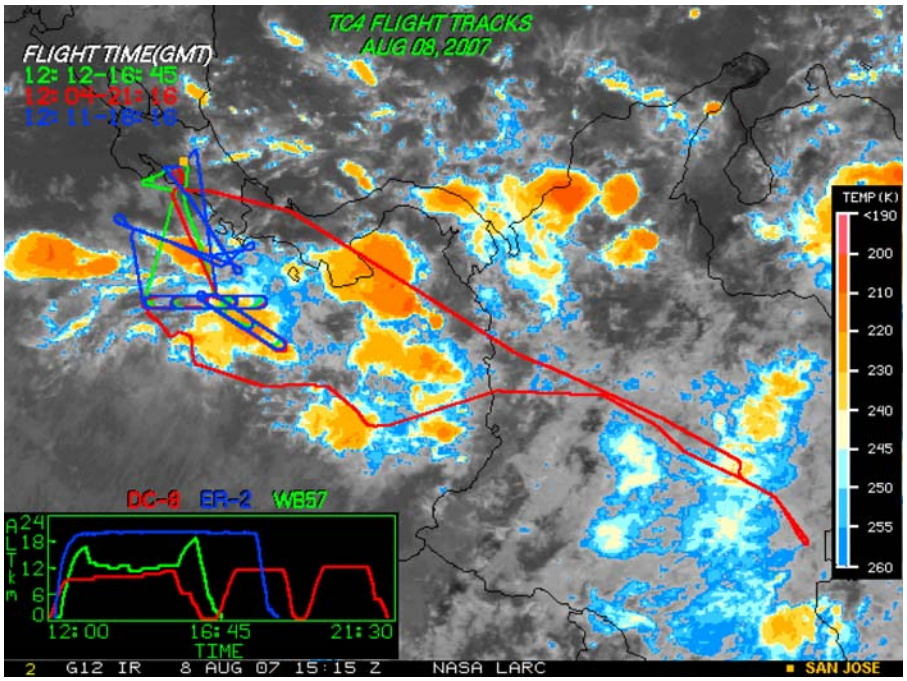

Figure 22. The flight tracks of the DC-8, ER-2, and WB-57F for 8 August 2007 superimposed on a GOES infrared brightness temperature image. For an explanation of the keys, see Figure 8. Base image is available at http://www-angler.larc.nasa.gov/tc4/flttrks/aug08/ALL_ALL.GOESIR.2007220.1528.gif.

the first measurements of solar and infrared heating rates in a subvisible cirrus. Radiative heating by subvisible cirrus is critical to the third mechanism for transport illustrated in Figure 2. The measured rates are consistent with previous calculations. An important aspect of the measurements is the technique used. It had been thought that either two aircraft, one above and one below the cloud, or one plane making long legs above and below would be needed to make the measurement, either of which is very costly in terms of flight time. However, it is found that a single aircraft could make the measurement by slowly descending through the cloud, which requires only moderate flight time, and could be combined with in situ measurements in the future.

[101] *Davis et al.* [2010] report on the properties of an extensive subvisible cirrus layer. This particular layer had very little mass, and would likely not be observed from satellites such as CALIPSO, suggesting that satellites may be underestimating the coverage of such clouds. They also summarize the properties of all the subvisible cirrus seen in TC4. Clouds with an optical depth below 0.03 and having a base above 15 km were seen 4% of the time during TC4. The typical subvisible cirrus contained quasi-spherical particles, had an optical depth near 0.007, was about 500 m thick, and was located a few hundred meters below the cold point tropopause. The particle size distributions, which are similar to those in previous campaigns, have an effective radius of about 14 μm and are very broad with substantial amounts of mass near 100 μm in diameter. Such broad size distributions are consistent with the clouds dehydrating the air just below the tropopause, which is consistent with the third mechanism in Figure 2.

6.4. Questions 4 and 5: What Controls Ozone in the TTl, and What Is the Fate of Short-Lived Boundary Layer Gases

[102] NO_x is an important ozone precursor. *Bucsela et al.* [2010] present case studies identifying lightning-generated upper tropospheric NO_x observed during TC4. Data from DC-8 aircraft missions within and near active storms and in relatively quiet areas were combine with corresponding data from the Ozone Monitoring Instrument (OMI) on the Earth Observing System Aura satellite to estimate the lightning-generated NO_2 (LNO_2) in the observed OMI NO_2 fields near storms. Information on lightning flashes, primarily cloud-to-ground (CG) flashes, observed by the surface networks operated by the Instituto Costarricense de Electricidad and the World Wide Lightning Location Network are examined over storms upwind of regions where OMI data indicates enhanced LNO_2. These flash data are compared with TRMM/LIS satellite overpass data to obtain the lightning detection efficiency for total flashes.

[103] *Bucsela et al.* [2010] use the NO_2/NO_x ratio estimated from the NASA Global Modeling Initiative model, to estimate the average NO_x (NO_2 + NO) production per lightning flash for each case in their study and obtained production rates in the range of 100–250 moles/flash, which are lower than rates derived from cloud-resolved chemistry modeling of storms observed in midlatitude experiments. The larger values of production per flash were estimates for storms in environments with stronger anvil-level winds. LIS flash footprint data that were available for one of the low-LNO_x production cases with weak upper tropospheric winds suggests shorter than typical flash lengths for this storm. *Bucsela*

et al. [2010] find that enhancements due to LNO_x over background determined from the OMI data were less than but roughly proportional to those estimated from the in situ aircraft data.

[104] It has long been thought that nitric acid is depleted in the upper troposphere by absorption onto ice cloud particle surfaces. *Scheuer et al.* [2010] present new DC-8 measurements of HNO_3 in cirrus clouds from anvil outflow made during TC4. Upper tropospheric (<9 km) measurements made during three flights while repeatedly traversing the same cloud region revealed depletions of gas-phase HNO_3 in regions characterized by higher ice water content and surface area. *Scheuer et al.* [2010] speculate that the depleted HNO_3 is due primarily to adsorption of HNO_3 onto cirrus ice surfaces. Using measurements of cirrus ice surface area density and some assumptions about background mixing ratios of gas phase HNO_3, they estimate molecular coverage of HNO_3 on cirrus ice surface in the tropical upper troposphere during the TC4 racetracks to be about 1×10^{13} molecules $\times$ cm^{-2}. While similar to measurements made during the NASA CRYSTAL-FACE campaign, this is somewhat less than predicted values stemming from recent laboratory experiments. *Scheuer et al.* [2010] also present an observation of considerably enhanced gas-phase HNO_3 at the base of a cirrus anvil suggesting vertical redistribution of HNO_3 by falling cirrus particles and subsequent particle sublimation and HNO_3 evaporation. The impact of released HNO_3, however, appears to be restricted to a very thin layer just below the cloud.

[105] Isotopes have proven to be important sources of information about the origins and fates of a number of chemical species in the atmosphere. *Croteau et al.* [2010] discuss vertical profiles of the oxygen and nitrogen isotopic compositions of N_2O from 500 m to 19 km from samples collected from the DC-8 and WB-57F during TC4. These profiles reveal the influence of a surface source at the lower altitudes and stratospheric photochemistry in the TTL and lower stratosphere. They are similar to profiles measured during CRAVE in January–February 2006. The coherent, predictable patterns measured show that, despite the large and often confounding variability in N_2O isotopic compositions on the scale of soil chamber or ocean sample measurements, these and future vertical profiles of N_2O isotopic compositions even at current measurement precisions can be used to constrain the N_2O isotope budget and the biogeochemical cycling of N_2O.

[106] *Avery et al.* [2010] examine the DC-8 in situ data from sampling in active convection and find a significant anticorrelation between in situ ozone and cloud total water content. Further, since there is little variability in boundary layer ozone in the convective donor region while there is a vertical gradient in ozone, low ozone in the upper troposphere can be used as a tracer for convective transport. The tracers peroxynitric acid (negative) and methyl hydrogen peroxide and bromine (positive) substantiate the results from using ozone as a tracer.

[107] Two case studies are shown by *Avery et al.* [2010] to demonstrate the ozone/cloud particle relationship, and then statistical distributions from all the available data in the upper troposphere are used to estimate the amount of convective turnover that has occurred below the tropical tropopause transition layer. The estimated amount of convective turnover is 50% in this region of the ITCZ, with the average height of convective outflow determined by a statistical minimum in the aggregate ozone profiles occurring at about 10 km. It appears that convective lofting in this region of the ITCZ is a two-stage process that mixes boundary layer air (ozone ~ 20 ppbv) up to an outflow region at 3–5 km, and then entrains air at 3–5 km and rapidly transports it to an outflow region located near 10 km.

[108] *Petropavlovskikh et al.* [2010] discuss an incident where very low ozone values were observed in the TTL during TC4. They examined the DC-8 in situ data and the remotely sensed data above the aircraft and inferred that the TTL was influenced by both slow ascent and by rapid transport due to deep convection. The transport trajectories and correlated measurements of ozone and boundary layer tracers suggest a strong connection between the deep convective processes regularly observed at low northern latitudes in July 2007 and the low-ozone episodes observed in the TTL near the coast of Ecuador. Back trajectory analyses indicate that the low-ozone features observed near the coast of Ecuador in the CAFS integrated ozone column and the DIAL ozone profile measurements aboard of the NASA DC-8 aircraft in July of 2007 was influenced by air with an origin in the equatorial eastern Pacific and/or Panama Bight regions. Because the ozone feature is so pronounced after 5–8 days of transit in the upper troposphere, it may provide information on mixing time scales in the TTL. Similar low ozone values in the TTL were seen in DIAL data during the PEM-A and PEM-B campaigns, however previous observations have not noted the low-ozone "bubble" seen during TC4.

[109] The ozonesondes from the SHADOZ sites at Costa Rica and San Cristobal (1.0S, 99W), along with daily launches from the NATIVE Panama location (7.8°N, 80°W), provide a fixed site perspective for viewing ozone structure in the TTL. The mean ozone profiles in the upper troposphere and lower TTL from Costa Rica and Panama display the characteristic "S shape" of most tropical SHADOZ sites [e.g., *Folkins et al.*, 2002] that was also observed over Mexico City during August 2006 [*Thompson et al.*, 2008]. The low-ozone segment corresponds to cloud outflow levels detected during TC4 sampling, e.g., with the ER-2 CPL and CRS imagery (D. Hlavka et al., Vertical cloud climatology during TC4 derived from high-altitude aircraft merged lidar and radar, submitted to *Journal of Geophysical Research*, 2010), as well as tracers from the DC-8. Analysis of stable ozone laminae in the Costa Rican and Panama sondes revealed a persistent pattern of convectively generated equatorial waves in the TTL [*Thompson et al.*, 2010, Figure 4].

[110] *Morris* [2010] present interesting observations of a strong convective complex formed in the Gulf of Panama east of Las Tablas on the morning of Sunday, 5 August 2007. World Wide Lightning Location Network data indicated 485 lightning flashes associated with this complex between 0800 and 1700 UT, with 398 of those flashes between 1200 and 1500 UT. At 1505 UT that day, an ozonesonde ascended into the southern edge of the now dissipating convective complex as it came ashore from the east and moved west across the Azuero Peninsula of Panama. Due to condensation on the balloon, down drafts associated with individual cells, or a combination of both, the balloon ascended through the 2 to 5 km region 5 times between 1512 and 1700, providing a truly unique examination of ozone production inside of a con-

vective complex. Ozone concentrations at these altitudes increased 4–12 ppb over the 108 min between the first and last ascent through these layers, yielding ozone production rates of 3–10 ppb/h and (assuming uniform production throughout the convective complex) ~2×10^6 moles of ozone. Using a photochemical model and data from the ER-2, WB-57, and DC-8, all of which flew in the vicinity of this convective complex, *Morris* [2010] are able to simulate the ozone production calculated using the balloon data.

[111] *Thornberry et al.* [2010] investigate the composition of aerosol residuals after heating to 300°C. The PALMS single particle mass spectrometer analyzed the composition of the nonvolatile fraction of the aerosols in a number of environments studied in TC4. The marine boundary layer, the free troposphere and the continental boundary layer over the Columbian jungle were studied. Sulfates were completely driven off by heating, except for sodium sulfate and related compounds in sea salt. Organic material in marine aerosols was less volatile than chlorine. Biomass aerosols survived heating better than sulfate-organic particles. For all of the particles there was a significant carbonaceous contribution other than elemental carbon.

6.5. Questions 6 and 7: What Controls Anvil Properties, and How Do They Evolve and Affect the Radiation Budget?

[112] Minnis et al. (submitted manuscript, 2010) provide an overview of the clouds that were seen from the GOES imagers and MODIS during TC4. The clouds over the TC4 domain (5°S–25°N, 70°W–100°W) vary dramatically over the diurnal cycle with maxima in clouds during the night over ocean and during the evening over land. The strongest convective activity occurs around the Isthmus of Panama with average ice water paths exceeding 700 g^{-2} over some areas during the experiment period (17 July to 8 August 2007). Stratus clouds cover much of the Pacific part of the domain at an average altitude around 1.5 km. The average coverage at night is roughly 30% greater than that during the day. Clouds over the Gulf of Mexico and Caribbean Sea were infrequent and thin, except over islands and coastlines.

[113] A long-standing controversy about anvil cirrus is the importance of ice crystals with sizes less than 50 μm. During the past decade a number of measurements have indicated that such sized crystals control the optical depths of clouds, and limit their sedimentation rate. However, it has been suggested that these small particles may not actually be so numerous in clouds as thought, but instead many may be created by the shattering of larger particles on the inlets of the sampling instruments [e.g., *McFarquhar et al.*, 2007]. TC4 used instruments that removed many of the surfaces on which shattering might occur, as well as standard instruments on which shattering might have occurred. *Jensen et al.* [2009a] show that indeed the vast majority of small particles are measurement artifacts for the clouds observed in TC4. The small particles that do exist contribute little to cloud extinction, radiative forcing, or radiative heating in the anvils.

[114] *Lawson et al.* [2010] discuss the size, shape and concentration of ice particles in tropical anvil cirrus and in situ cirrus clouds as measured with a 2D-S probe, an optical imaging probe with improved response characteristics and the ability to remove shattered artifacts. The data were collected with the DC-8 and WB-57F research aircraft near Costa Rica during TC4, and with the DC-8 near Cape Verde during the 2006 NASA African Monsoon Multidisciplinary Analyses (NAMMA) campaign.

[115] *Lawson et al.* [2010] collected data in convective turrets, anvils still attached to convection, aged anvils detached from convection and cirrus formed in situ. Unusually strong maritime convection was encountered, with peak updrafts of 20 m s^{-1}, ice water contents exceeding 2 g m^{-3} and total particle concentrations exceeding 10 cm^{-3} at 12.2 km. Ice water contents in the anvils declined outward from the center of convection, decreasing to <0.1 g m^{-3} in aged anvil cirrus. The data show that microphysical and radiative properties of both tropical anvils and cirrus are most strongly influenced by ice particles in the size range from about 100 to 400 μm. This is contrary to several previous investigations that have suggested that ice particles less than about 50 μm control radiative properties in anvils and cirrus.

[116] *Lawson et al.* [2010] input 2D-S particle area and mass size distributions, plus information on particle shape, into an optical properties routine that computes cloud extinction, asymmetry parameter and single scattering albedo. These optical properties were then input into a two-stream radiative code to compute radiative heating profiles within the various cloud types. The results produce short- and long-wave heating/cooling vertical profiles in these tropical clouds. A simple parameterization based on 2D-S measurements is derived from the particle mass size distribution that yields an area size distribution. The parameterized area size distribution can then be used in large-scale numerical simulations that include radiative transfer packages.

[117] *Tian et al.* [2009] examine 2 days of in situ observations of ice particle size spectra in convectively generated cirrus to determine if the data was well fit to exponential, gamma or lognormal function size distributions. They show that transformed exponential, gamma and lognormal distributions should collapse onto standard curves. An examination of the transformed spectra, and of deviations of the transformed spectra from the standard curves, shows that the lognormal function provides the best fit to the observed spectra.

[118] A difficult issue in remote sensing of clouds is to determine the cloud top and base heights, and to detect multiple cloud layers. Depending on the wavelength and technique used remote sensing instruments penetrate to different depths. Hlavka et al. (submitted manuscript, 2010) address this issue using a lidar and radar on the ER-2. Among other goals they compile statistical data on cloud location. Hlavka et al. (submitted manuscript, 2010) find that the TC4 Study Area was very cloudy, with clouds occurring 94% of the time in vertical profiles. One to three cloud layers were common, with the average calculated at 2.03 layers per profile. The cloud frequency in the upper troposphere averaged 42%. There were regional differences. The Caribbean had fewer clouds than the other regions. High clouds occurred over land more frequently than over ocean areas. The Panama Gulf region had the highest probability of clouds throughout the vertical column. The average height above the ground where the cumulative optical depth (starting at 20 km) reached 1.0 was 5.968 km and where it reached 3.0 was 4.258 km.

[119] P. Kucera and A. J. Newman (Characteristics of convection observed over Panama and adjacent Gulf of

Panama during TC4, manuscript in preparation, 2010) examine the characteristics of convection over the southern peninsula of Panama and adjacent Gulf of Panama using data from the NASA 10 cm polarimetric Doppler weather radar (NPOL) and rainfall measurements obtained from a high-resolution rain gauge network. A variety of events were observed during TC4. Events ranged from short-lived unorganized convection to long-lived mesoscale convective systems (MCSs). Results show that organized systems often developed and intensified over the Gulf of Panama in the late evening before weakening and dissipating prior to reaching land in the midmorning hours. A secondary peak in convection as a result of strong diurnal heating was observed over the mountainous region of Panama during midafternoon. Analysis of the vertical structure of the storms was nearly the same for evening and morning with slightly more deep convection in late afternoon.

[120] Whether clouds absorb more sunlight than would be expected, or not, has been an issue for many years. *Schmidt et al.* [2010] shed light on this problem using TC4 data. Coordinated flight legs of the ER-2 and DC-8 aircraft flying above and below extended cirrus layers played an important part in TC4. The Solar Spectral Flux Radiometer (SSFR) measured upward and downward irradiance on both aircraft, which allowed the so-called apparent absorption to be determined on a point-by-point basis along the flight track. Apparent absorption is defined as the difference in net flux on top and at the bottom of a cloud. It is not a good proxy for the real absorption for highly heterogeneous cloud scenes where horizontal photon transport through the sides of the sampling volume is an important contributor to flux divergence. *Schmidt et al.* [2010] show, for the first time, measured spectral apparent absorption. They compare the data with results from a three-dimensional radiative transfer model. The modeled cloud field was generated from optical thickness and effective ice crystal radius retrievals from the MODIS Airborne Simulator (MAS), and from reflectivity profiles from the Cloud Radar System (CRS), both onboard the ER-2. *Schmidt et al.* [2010] find considerable apparent absorption in areas of relatively high optical thickness, for both visible wavelengths (where clouds do not absorb) and in the near-infrared ice absorption bands. This absorption is well reproduced by the model results. The fact that photons are effectively redistributed from optically thick to optically thin regions supports previous studies where observed absorption biases were attributed to undersampling of the clear areas around clouds. The spectral signature of the bias may have implications for cloud remote sensing; studying this new effect in greater detail thus appears to be important in future cloud experiments.

[121] *Heymsfield et al.* [2009] compare Doppler radar observations of the strength of vertical motions in convection from a wide variety of field missions including TC4. They find that strong updrafts, most exceeding 15 m s^{-1} with a few exceeding 30 m s^{-1}, are found in all the deep convection cases, whether over land or ocean. They also find that peak updrafts were almost always above the 10 km level and in the case of tropical cyclones, closer to the 12 km level. In addition, tropical convection often has double-peaked updraft velocities with the smaller peak at lower levels and the larger peak at higher altitudes. Finally, land-based and sea breeze convection had higher reflectivities, slightly higher vertical velocities, and wider convective cores than oceanic and tropical cyclone convection. *Heymsfield et al.* [2009] discuss their results in terms of dynamical and microphysical implications for numerical models and future remote sensors.

[122] *Bedka and Minnis* [2010] explore GOES data during TC4. Their results show clear differences in the areal coverage of anvil cloud, deep convection, and overshooting deep convective cloud tops (OT) over land and water and also throughout the diurnal cycle. The offshore waters of Panama, northwest Colombia, and El Salvador were the most active regions for OT-producing storms. Most OT clouds occurred during the evening and night. A convective cloud object tracking system is used to monitor the duration and areal coverage of storm complexes as well as the time evolution of their cloud top microphysical properties. The mean lifetime for these complexes is 5 h with some existing for longer than 20 h. *Bedka and Minnis* [2010] find deep convection within the anvil cloud during 60% of the storm lifetime and covering 24% of the anvil cloud. The cloud top heights and optical depths at the storm core follow a reasonable pattern with maximum values occurring 20% into the storm lifetime. The values in the surrounding anvil cloud peaked at a relative age of 20–50% before decreasing as the convective system decays. Ice particle diameter decreased with distance from the core but generally increased with storm age. These results, which characterize the average convective system during the experiment, should be valuable for formulating and validating convective cloud process models.

[123] *Parodi and Tanelli* [2010] used the Weather Research Forecasting (WRF) model to conduct high-resolution numerical simulations of deep moist convective processes observed during TC4, over the East Pacific Inter-Tropical Convergence Zone. Three different turbulent closures, and two microphysical parameterizations are used. Their impact on the spatial-temporal structure of predicted convective fields is compared to TC4 observations from geostationary imager, airborne precipitation radar and dropsondes. It is found that the large eddy simulation (LES) turbulent closure "upscaled" to the terra incognita range of grid spacings (i.e., 0.1–1 km) is best suited to model the deep convective processes under examination.

6.6. Question 8: How Can Space-Based Measurements of Geophysical Parameters Be Validated?

[124] *Kindel et al.* [2010] discuss the important issue of the accuracy of satellite retrieval of cloud optical properties. They retrieve the cirrus cloud optical depth and effective radius from hyperspectral irradiance and discrete spectral radiance measurements for four cirrus cloud cases during TC4 over a range of solar zenith angle (23° to 53°) and high (46–90) and low (5–15) optical thicknesses. The retrieved optical depth and effective radius using measurements at only two wavelengths from the Solar Spectral Flux Radiometer (SSFR) Irradiance and the MODIS airborne simulator (MAS) is input to a radiative transfer model using two libraries of ice crystal single scattering optical properties to reproduce spectral albedo over the spectral range from 400 to 2130 nm. The two commonly used ice single scattering models are evaluated by examining the residuals between observed spectral and predicted spectral albedo. The SSFR and MAS retrieved optical

depth and effective radius are in close agreement for the low to moderately optically thick clouds with a mean difference of 2.76 in optical depth (SSFR lower relative to MAS) and 2.25 mm in effective radius (MAS smaller relative to SSFR). The higher optical depth case exhibits a larger difference in optical depth (40.5) but nearly identical results for effective radius. The single scattering libraries are capable of reproducing the spectral albedo in most cases examined to better than 0.05 for all wavelengths. Systematic differences between the model and measurements increase with increasing optical thickness and approached 0.10 between 400 and 600 nm and selected wavelengths between 1200 and 1300 nm. Differences between radiance- and irradiance-based retrievals of optical thickness and effective radius error sources in the modeling of ice single scattering properties are examined.

[125] H. Eichler et al. (Relative impact of cloud heterogeneities and scattering phase function on remotely sensed cirrus optical thickness and effective crystal radius, submitted to *Journal of Geophysical Research*, 2010) evaluate the relative impact of ice crystal scattering phase function and three-dimensional (3D) effects in heterogeneous cirrus clouds on remote sensing products (optical thickness and effective crystal radius). Their study is based on 3D and independent pixel approximation (IPA) radiative transfer model calculations, using an input cloud that was generated from data collected during TC4. In current ice cloud retrievals from satellite imagers using unpolarized light, the scattering phase function has to be assumed a priori. The various effects of cloud heterogeneities are ignored in current techniques. Both simplifications introduce errors in the retrievals. Eichler et al. (submitted manuscript, 2010) calculate spectral upwelling radiance fields from the input cloud as they would be sensed from space or aircraft. They thereby use the same ice cloud properties that are the basis for satellite retrievals from the Moderate Resolution Imaging Spectroradiometer (MODIS). Eichler et al. (submitted manuscript, 2010) then retrieve the optical thickness and crystal effective radius that would be obtained in standard satellite techniques under the IPA assumption. The ratios between the retrieved and the original fields are used as a metric for cloud heterogeneity effects on retrievals. To estimate the error that arises from inappropriate choices of phase functions, Eichler et al. (submitted manuscript, 2010) retrieve optical thickness and crystal effective radius using different phase functions than the set that was used for calculating the radiance fields. The ratio between retrieved and original values of optical thickness and effective radius serve as metric for phase function effects. Eichler et al. (submitted manuscript, 2010) then compare the two types of ratios (heterogeneity effect and scattering phase function effect) and found that both are of the same magnitude, with different dependencies on optical thickness, effective radius, and optical thickness variability. Eichler et al. (submitted manuscript, 2010) find positive and negative biases of up to 50% for both optical thickness and crystal effective radius. Cloud heterogeneities cause optical thickness to be underestimated and effective radius to be overestimated in optically thick regions. The phase function ratios are constant with cloud optical thickness, but the retrieval bias of effective radius may increase or decrease with crystal size, depending on the scattering phase function.

[126] *Yost et al.* [2010] compare cloud properties derived using radiance measurements from the GOES imagers to similar quantities from aircraft in situ observations and search for meaningful relationships in the data. A new method using dual-angle satellite measurements is used to derive the ice water content (IWC) for the top portion of deep convective clouds and anvils. The results show the in situ and remotely sensed mean particle sizes agree to within ~10 μm in the top few kilometers of thick anvils despite the vastly different temporal and spatial resolutions of the aircraft and satellite instruments. Mean particle size and IWC are shown to increase with decreasing altitude in the top few kilometers of the cloud. Given these relationships, it is possible to derive parameterizations for effective particle size and IWC as a function of altitude from satellite observations.

[127] *Chang et al.* [2010] discuss cloud top heights. They evaluate four techniques to determine cloud top height from GOES data, which they compare against the ER-2 cloud lidar data (CPL). The CPL detected 89% coverage by upper tropospheric clouds, while the retrievals from GOES suggest 76, 76, 69, and 74%. Most of the differences are due to very thin cirrus. Many subvisible thin layer clouds near the tropopause are detected only by the CPL. The mean upper tropospheric cloud top heights for the 9 days studied are 14.2 (±2.1) km for the CPL and 10.7 (±2.1), 12.1 (±1.6), 9.7 (±2.9)44 and 11.4 (±2.8) km for the various GOES analyses. The biases for all techniques increase with increasing numbers of cloud layers. The transparency of the upper layer cloud(s) tends to increase with the numbers of cloud layers.

[128] S. A. Carn et al. (In-situ sampling of tropospheric volcanic plumes in Ecuador and Columbia during TC4, manuscript in preparation, 2010) describe in situ measurements of SO_2 in volcanic plumes and compare with those from the OMI instrument on the Aura satellite. The DC-8 aircraft penetrated tropospheric gas and aerosol plumes sourced from active volcanoes in Ecuador and Colombia during TC4. The emissions originated from Tungurahua volcano (Ecuador; altitude 5023 m), an open-vent system that has exhibited near-continuous unrest since 1999, and Nevado del Huila (Colombia; altitude 5365 m), a heavily glaciated volcano that reactivated in February 2007 after several centuries of dormancy. Elevated concentrations of SO_2, sulfate aerosol and particles were measured by instrumentation aboard the DC-8 in layers of probable volcanic origin at altitudes of 3–6 km. Comparisons with operational OMI SO_2 (OMSO2) data reveal that SO_2 column contents measured in the Tungurahua plume (~0.1–0.2 DU) were too low for detection in individual OMI IFOV data, but are in agreement with average SO_2 columns measured by OMI in the volcanic outflow region in July 2007. Higher SO_2 amounts (~100 ppbv) were measured in the Huila plume on 21 July. A 3–4 h time difference between the DC-8 sampling of the Huila plume and the Aura overpass requires modeling of plume transport and chemistry before the measurements can be compared. Generally the SO_2 measured by the aircraft is consistent with that reported by OMI.

[129] *King et al.* [2010] compare ER-2 aircraft observations with those of MODIS and MISR on the Terra spacecraft, both of which were over extensive marine stratocumulus clouds composed exclusively of liquid water droplets. In these comparisons, the probability density functions of cloud optical thickness and effective radius are nearly identical, providing further confidence in the ability of MODIS to

derive cloud optical properties over extensive liquid water clouds over the ocean.

7. Summary

[130] TC4 addressed each of the goals it set out to consider (Table 1). Within the context of related missions and NASA's satellite program, we are significantly closer to answering some of these fundamental questions. While the late arrival of the WB-57F compromised our ability to obtain as much high-altitude in situ data as we originally planned, we were fortunate that the DC-8 had a sophisticated instrument package and was able to meet many of the goals originally set for the WB-57F. We were able to make three flights with the set of three aircraft, which did provide a considerable amount of useful data over the full range of altitudes.

[131] The execution of the TC4 field mission was a significant advance over many previous missions because of our ability to control the aircraft in real time. We often changed the flight plans so that the aircraft were able to sample convective systems as they evolved. It was common for the locations of convective complexes to be significantly different between the forecasts and reality, for example for convection to be in the Pacific rather than in the Caribbean. These differences required us to alter flight plans in significant ways just after takeoff. In addition, convective cores can appear within minutes, and convective complexes dissipate over time. Therefore, we had to alter flight plans in real time to keep the aircraft away from dangerous portions of the clouds, but also to take data in the interesting portions of the clouds such as anvils. We also were able to use data from the aircraft in real time to maximize the locations of the aircraft relative to interesting phenomena. For example, by using lidar data showing the locations of cloud and aerosol layers, we were able to alter the aircraft altitude to probe these layers, which normally would not have been identified until after the mission. The ability to control the aircraft in flight has been developing for some time, but this is the first mission where the three NASA aircraft had mechanisms to track all of them, and to downlink data. This advance converts aircraft research into an experimental framework, in which questions can be asked and addressed in real time and phenomena probed in greater detail than before when they were identified only in forecasts.

[132] **Acknowledgments.** The TC4 mission was supported by the Atmospheric Composition research area of NASA's Earth Science Division. We thank the aircraft managers, engineers, and ground crews of all the aircraft that participated in TC4. We particularly thank the pilots of the ER-2, David Wright, Denis Steele, and DeLewis Porter, and Mobile Pilot Jan Nystrom, the WB-57F pilots Rob Rivers, Scott Reagan, and William Rieke, and Backseaters, John Bain, Dominic Del Russo, and Joseph Gerky, and the DC-8 pilots William Brocket, Mike Fuller, Manny Puerta, and the late Edwin Lewis. The ER-2 aircraft and pilots were very well supported by the personnel of NASA's Dryden Flight Research Center Airborne Science Directorate, the WB-57F by NASA's Johnson Space Center High Altitude Research Program, and the DC-8 by the University of North Dakota's National Science Education Research Center. We thank the ER-2 Aircraft Program Director, Robert Curry, the DC-8 Program Director, Rick Shetter, and the WB-57F Program Manager, Ken Cockrell. We also thank the ER-2 aircraft coordinators Jacques Vachon and Mike Kapitzke, the DC-8 Aircraft Manager Steve Davis and the DC-8 Mission Manager Dave Easmunt, and the WB-57F Program Engineers Shelly Baccus and Frank Caldeiro, the Mission Manager William (Bud) Meins, and the Integration Manager Marty Ross, as well as all of the aircraft crews. The NASA Ames Earth Science Project Office made tremendous contributions to the operations and overall success of TC4. Our special thanks go to Kent Schiffer, Mike Gaunce, Sue Tolley, Quincy Allison, Dan Chirica, and the late Steve Gaines. We also appreciate the support of the NPOL radar, NATIVE trailer, and Sat Com groups in Panama and the SMART mobile radar in Costa Rica. We thank the RTMM and REVEAL teams from NASA Marshall Earth Science Office and NASA Dryden Test Systems Directorate, respectively, for enabling the collection and display of airborne and ground-based data sets, which supported mission planning and enabled critical real-time decision making. The shipment of the tons of science hardware to San Jose, Costa Rica, could not have been accomplished without the tremendous efforts of the U.S. Air Force Material Command. We would also like to thank the pilots and staff of the NASA C-9, NASA G-3, and Beale Air force Base KC-135 for all their support. We would like to record our special appreciation of and thanks to Kathy Thompson for her dedication and effort throughout the planning, operation, and postmission analysis of TC4. Kathy was ably assisted by Rose Kendall, to whom we also send our thanks. Tommy Thompson's myriad skills were critical to the successful operation of the mission in the field. We thank him for being there to make sure, once again, that it all worked. The airport personnel at Juan Santamaria airport were very helpful to the mission. The various Costa Rican government, academic, and commercial organizations we worked with, including CeNAT, DGAC, Alterra, ICE, IMN, ADS, and the Servicio de Vigilancia Aerea, were invaluable. The same can be said for the Panamanian government and academic organizations. The Costa Rican National Center for Advanced Technology (CENAT), and especially Oliver Gómez, were instrumental in logistical support, both before and during the mission. The meteorological forecasting team in Costa Rica was critical to the success of TC4. This was a joint effort of the Instituto Meteorológico Nacional (IMN), the Centro de Investigaciones Geofisicas (CIGEFI) at the University of Costa Rica, and the Instituto Costarricense de Electricidad (ICE). IMN team members were Evelyn Quirós Badilla, Gustavo Murillo Zumbado, and Eladio Solano León; the CIGEFI group, under the direction of Jorge Amador, included Erick Rivera Fernández, Marcela Ulate Medrano, Ana María Duran Quesada, and Blanca Calderón Solera, and Berny Fallas López represented ICE. NASA Headquarters management and program managers supported this mission in many meaningful ways. The U.S. Embassies in Costa Rica and Panama were especially helpful in coordinating this effort. We appreciate the hospitality of Costa Rican Ambassador Mark Langdale. We appreciate the help of the people of Panama who facilitated the use of the NATIVE trailer and the NPOL radar, and the people of the Galapagos who helped with balloon launching. We especially thank the President and people of Costa Rica, who reconstructed the hangar used by the WB-57F, loaned us the President's hangar for the ER-2, and were very friendly, helpful, and hospitable.

References

Avery, M., J. Joiner, C. Twohy, G. Diskin, G. Sachse, P. Lawson, M. McGill, and K. Severance (2010), Convective distribution of tropospheric ozone and tracers in the Central American ITCZ region: Evidence from observations during TC4, *J. Geophys. Res.*, doi:10.1029/2009JD013450, in press.

Bedka, K. M., and P. Minnis (2010), GOES-12 observations of convective storm variability and evolution during the TC4 field program, *J. Geophys. Res.*, doi:10.1029/2009JD013227, in press.

Boehm, M. T., and J. Verlinde (2000), Stratospheric influence on upper tropospheric tropical cirrus, *Geophys. Res. Lett.*, *27*, 3209–3212, doi:10.1029/2000GL011678.

Bucholtz, A., D. L. Hlavka, M. J. McGill, K. S. Schmidt, P. Pilewskie, S. M. Davis, E. A. Reid, and A. L. Walker (2010), Directly measured heating rates of a tropical subvisible cirrus cloud, *J. Geophys. Res.*, doi:10.1029/2009JD013128, in press.

Bucsela, E., et al. (2010), Lightning-generated NO_x seen by OMI during NASA's TC4 experiment, *J. Geophys. Res.*, doi:10.1029/2009JD013118, in press.

Chang, F.-L., P. Minnis, J. K. Ayers, M. J. McGill, R. Palikonda, D. A. Spangenberg, W. L. Smith Jr., and C. R. Yost (2010), Evaluation of satellite-based upper troposphere cloud-top-height retrievals in multilayer cloud conditions during TC4, *J. Geophys. Res.*, doi:10.1029/2009JD013305, in press.

Comstock, J. M., T. P. Ackerman, and G. G. Mace (2002), Ground-based remote sensing of tropical cirrus clouds at Nauru Island: Cloud statistics and radiative impacts, *J. Geophys. Res.*, *107*(D23), 4714, doi:10.1029/2002JD002203.

Corti, T., B. P. Luo, Q. Fu, H. Vömel, and T. Peter (2006), The impact of cirrus clouds on tropical troposphere-to-stratosphere transport, *Atmos. Chem. Phys.*, *6*, 2539–2547, doi:10.5194/acp-6-2539-2006.

Corti, T., et al. (2008), Unprecedented evidence for deep convection hydrating the tropical stratosphere, *Geophys. Res. Lett.*, *35*, L10810, doi:10.1029/2008GL033641.

Croteau, P., E. Atlas, S. M Schauffler, D. R Blake, G. S. Diskin, and K. A. Boering (2010), Effect of local and regional sources on the isotopic composition of nitrous oxide in the tropical free troposphere and tropopause layer, *J. Geophys. Res.*, doi:10.1029/2009JD013117, in press.

Davis, S., D. Hlavka, E. Jensen, K. Rosenlof, S. Schmidt, S. Borrmann, W. Frey, H. Voemel, and T. P. Bui (2010), In situ and lidar observations of subvisible clouds during TC4, *J. Geophys. Res.*, doi:10.1029/2009JD013093, in press.

DeMott, P. J., K. Sassen, M. R. Poellet, D. Baumgardner, D. C. Rogers, S. D. Brooks, A. J. Prenni, and S. M. Kreidenweis (2003), African dust aerosols as atmospheric nuclei, *Geophys. Res. Lett.*, *30*(14), 1732, doi:10.1029/2003GL017410.

Dessler, A. E., T. F. Hanisco, and S. Fueglistaler (2007), Effects of convective ice lofting on H_2O and HDO in the tropical tropopause layer, *J. Geophys. Res.*, *112*, D18309, doi:10.1029/2007JD008609.

Dvortsov, V. L., M. A. Geller, S. Solomon, S. M. Schauffler, E. L. Atlas, and D. R. Blake (1999), Rethinking halogen budgets in the midlatitude lower stratosphere, *Geophys. Res. Lett.*, *26*, 1699–1702, doi:10.1029/1999GL900309.

Folkins, I., P. O. Wennberg, T. F. Hanisco, J. G. Anderson, and R. J. Salawitch (1997), OH, HO_2, and NO in two biomass burning plumes: Sources of HO_x and implications for ozone production, *Geophys. Res. Lett.*, *24*, 3185–3188, doi:10.1029/97GL03047.

Folkins, I., M. Loewenstein, J. Podolske, S. J. Oltmans, and M. Proffitt (1999), A barrier to vertical mixing at 14 km in the tropics: Evidence from ozonesondes and aircraft measurements, *J. Geophys. Res.*, *104*, 22,095–22,102, doi:10.1029/1999JD900404.

Folkins, I., C. Braun, A. M. Thompson, and J. C. Witte (2002), Tropical ozone as in indicator of deep convective outflow, *J. Geophys. Res.*, *107*(D13), 4184, doi:10.1029/2001JD001178.

Forster, P. M., and K. P. Shine (2002), Assessing the climate impact of trends in stratospheric water vapor, *Geophys. Res. Lett.*, *29*(6), 1086, doi:10.1029/2001GL013909.

Fridlind, A. M., A. S. Ackerman, and E. J. Jensen (2004), Evidence for the predominance of mid-tropospheric aerosols as subtropical anvil cloud nuclei, *Science*, *304*, 718–722, doi:10.1126/science.1094947.

Fueglistaler, S., and P. H. Haynes (2005), Control of interannual and longer-term variability of stratospheric water vapor, *J. Geophys. Res.*, *110*, D24108, doi:10.1029/2005JD006019.

Fueglistaler, S., A. E. Dessler, T. J. Dunkerton, I. Folkins, Q. Fu, and P. W. Mote (2009), Tropical tropopause layer, *Rev. Geophys.*, *47*, RG1004, doi:10.1029/2008RG000267.

Gao, R. S., et al. (2004), Evidence that nitric acid increases relative humidity in low-temperature cirrus clouds, *Science*, *303*, 516–520, doi:10.1126/science.1091255.

Gettelman, A., and P. M. D. F. Forster (2002), A climatology of the tropical tropopause layer, *J. Meteorol. Soc. Jpn.*, *80*, 911–924, doi:10.2151/jmsj.80.911.

Gettelman, A., W. J. Randel, F. Wu, and S. T. Massie (2002), Transport of water vapor in the tropical tropopause layer, *Geophys. Res. Lett.*, *29*(01), 1009, doi:10.1029/2001GL013818.

Gettelman, A., P. M. D. F. Forster, M. Fujiwara, Q. Fu, H. Vömel, L. K. Gohar, C. Johanson, and M. Ammerman (2004), Radiation balance of the tropical tropopause layer, *J. Geophys. Res.*, *109*, D07103, doi:10.1029/2003JD004190.

Hartmann, D. L., J. R. Holton, and Q. Fu (2001), The heat balance of the tropical tropopause, cirrus, and stratospheric dehydration, *Geophys. Res. Lett.*, *28*, 1969–1972, doi:10.1029/2000GL012833.

Heymsfield, G. M., L. Tian, A. J. Heymsfield, L. Li, and S. Guimond (2009), Characteristics of deep tropical and sub-tropical convection from nadir-viewing high-altitude airborne Doppler radar, *J. Atmos. Sci.*, *67*, 285–308.

Highwood, E. J., and B. J. Hoskins (1998), The tropical tropopause, *Q. J. R. Meteorol. Soc.*, *124*, 1579–1604, doi:10.1002/qj.49712454911.

Holton, J., and A. Gettelman (2001), Horizontal transport and dehydration of the stratosphere, *Geophys. Res. Lett.*, *28*, 2799–2802, doi:10.1029/2001GL013148.

Holton, J. R., P. H. Haynes, M. E. Mcintyre, A. R. Douglas, R. B. Rood, and L. Pfister (1995), Stratosphere-troposphere exchange, *Rev. Geophys.*, *33*, 403–439, doi:10.1029/95RG02097.

Jacob, D. J., J. H. Crawford, M. M. Kleb, V. S. Connors, R. J. Bendura, J. L. Raper, G. W. Sachse, J. C. Gille, L. Emmons, and C. L. Heald (2003), The Transport and Chemical Evolution over the Pacific (TRACE-P) aircraft mission: Design, execution, and first results, *J. Geophys. Res.*, *108*(D20), 9000, doi:10.1029/2002JD003276.

Jaeglé, L., et al. (1997), Observed OH and HO_2 in the upper troposphere suggest a major source from convective injection of peroxides, *Geophys. Res. Lett.*, *24*, 3181–3184, doi:10.1029/97GL03004.

Jenkins, G. S., K. Mohr, V. R. Morris, and O. Arino (1997), The role of convective processes over the Zaire-Congo basin to the southern hemispheric ozone maximum, *J. Geophys. Res.*, *102*, 18,963–18,980, doi:10.1029/97JD01018.

Jensen, E. J., and L. Pfister (2004), Transport and freeze-drying in the tropical tropopause layer, *J. Geophys. Res.*, *109*, D02207, doi:10.1029/2003JD004022.

Jensen, E. J., O. B. Toon, H. B. Selkirk, J. D. Spinhirne, and M. R. Schoeberl (1996), On the formation and persistence of subvisible cirrus clouds near the tropical tropopause, *J. Geophys. Res.*, *101*, 21,361–21,375, doi:10.1029/95JD03575.

Jensen, E. J., D. Starr, and O. B. Toon (2004), Mission investigates tropical cirrus clouds, *Eos Trans. AGU*, *85*, 45–50.

Jensen, E. J., et al. (2005), Ice supersaturations exceeding 100% at the cold tropical tropopause: Implications for cirrus formation and dehydration, *Atmos. Chem. Phys.*, *5*, 851–862, doi:10.5194/acp-5-851-2005.

Jensen, E. J., A. S. Ackerman, and J. A. Smith (2007), Can overshooting convection dehydrate the tropical tropopause layer?, *J. Geophys. Res.*, *112*, D11209, doi:10.1029/2006JD007943.

Jensen, E. J., et al. (2008), Formation of large (100 μm) ice crystals near the tropical tropopause, *Atmos. Chem. Phys.*, *8*, 1621–1633, doi:10.5194/acp-8-1621-2008.

Jensen, E. J., et al. (2009a), On the importance of small ice crystals in tropical anvil cirrus, *Atmos. Chem. Phys. Discuss.*, *9*, 5321–5370, doi:10.5194/acpd-9-5321-2009.

Jensen, E. J., et al. (2009b), Ice nucleation and cloud microphysical properties in tropical tropopause layer cirrus, *Atmos. Chem. Phys. Discuss.*, *9*, 20,631–20,675, doi:10.5194/acpd-9-20631-2009.

Kindel, B. C., K. Sebastian, P. Pilewskie, B. Baum, P. Yang, and S. Platnick (2010), Observations and modeling of ice cloud shortwave spectral albedo during the Tropical Composition, Cloud and Climate Coupling Experiment, *J. Geophys. Res.*, doi:10.1029/2009JD013127, in press.

King, M. D., S. Platnick, G. Wind, G. T. Arnold, and R. T. Dominguez (2010), Remote sensing of radiative and microphysical properties of clouds during TC4: Results from MAS, MASTER, MODIS, and MISR, *J. Geophys. Res.*, doi:10.1029/2009JD013277, in press.

Kley, D., P. J. Crutzen, H. G. J. Smit, H. Vömel, S. J. Oltmans, H. R. Grassl, and V. Ramanathan (1996), Observations of near-zero ozone concentrations over the convective Pacific—Effects on air chemistry, *Science*, *274*, 230–233, doi:10.1126/science.274.5285.230.

Ko, M. K. W., and G. Poulet (2002), Very-short halogen and sulfur substances, in *Scientific Assessment of Ozone Depletion: 2002*, chap. 2, UNEP, Nairobi.

Ko, M. K. W., N. D. Sze, C. J. Scott, and D. K. Weisenstein (1997), On the relation between stratospheric chlorine/bromine loading and short-lived tropospheric source gases, *J. Geophys. Res.*, *102*, 25,507–25,517, doi:10.1029/97JD02431.

Komhyr, W. D., R. A. Barnes, G. B. Brothers, J. A. Lathrop, and D. P. Opperman (1995), Electrochemical concentration cell ozonesonde performance during STOIC, *J. Geophys. Res.*, *100*, 9231–9244, doi:10.1029/94JD02175.

Krämer, M., et al. (2009), Ice supersaturations and cirrus cloud crystal numbers, *Atmos. Chem. Phys.*, *9*, 3505–3522, doi:10.5194/acp-9-3505-2009.

Lawson, R. P., E. J. Jensen, D. L. Mitchell, B. Baker, Q. Mo, and B. Pilson (2010), Microphysical and radiative properties of tropical clouds investigated in TC4 and NAMMA, *J. Geophys. Res.*, doi:10.1029/2009JD013017, in press.

Liu, C., and E. J. Zipser (2005), Global distribution of convection penetrating the tropical tropopause, *J. Geophys. Res.*, *110*, D23104, doi:10.1029/2005JD006063.

Liu, C., and E. J. Zipser (2009), Implications of the day versus night differences of water vapor, carbon monoxide, and thin cloud observations near the tropical tropopause, *J. Geophys. Res.*, *114*, D09303, doi:10.1029/2008JD011524.

Logan, J. A. (1999), An analysis of ozonesonde data for the troposphere: Recommendations for testing 3-D models, and development of a gridded climatology for tropospheric ozone, *J. Geophys. Res.*, *104*, 16,115–16,149, doi:10.1029/1998JD100096.

Luo, Z., and W. B. Rossow (2004), Characterizing tropical cirrus life cycle, evolution, and interaction with upper-tropospheric water vapor using Lagrangian trajectory analysis of satellite observations, *J. Clim.*, *17*, 4541–4564, doi:10.1175/3222.1.

Mace, G. G., M. Deng, B. Soden, and E. Zipser (2006), Association of tropical cirrus in the 10–15 km layer with deep convective sources: An observational study combining millimeter radar data and satellite-derived trajectories, *J. Atmos. Sci.*, *63*, 480–503, doi:10.1175/JAS3627.1.

McFarquhar, G. M., A. J. Heymsfield, J. Spinhirne, and B. Hart (2000), Thin and subvisual tropopause cirrus: Observations and radi-

ative impacts, *J. Atmos. Sci.*, *57*, 1841–1853, doi:10.1175/1520-0469(2000)057<1841:TASTTC>2.0.CO;2.

McFarquhar, G. M., J. Um, M. Freer, D. Baumgardner, G. L. Kok, and G. Mace (2007), Importance of small crystals to cirrus properties: Observations from the Tropical Warm Pool International Cloud Experiment (TWP-ICE), *Geophys. Res. Lett.*, *34*, L13803, doi:10.1029/2007GL029865.

McKeen, S. A., T. Gierczak, J. B. Burkholder, P. O. Wennberg, T. F. Hanisco, E. R. Keim, R. S. Gao, S. C. Liu, A. R. Ravishankara, and D. W. Fahey (1997), The photochemistry of acetone in the upper troposphere - a source of odd-hydrogen radicals, *Geophys. Res. Lett.*, *24*, 3177–3180, doi:10.1029/97GL03349.

Morris, G. (2010), Observations of ozone production in a dissipating tropical convective cell during TC4, *J. Geophys. Res.*, doi:10.1029/2010JD014098, in press.

Mote, P. W., K. H. Rosenlof, M. E. McIntyre, E. S. Carr, J. C. Gille, J. R. Holton, J. S. Kinnersley, H. C. Pumphrey, J. M. Russell, and J. W. Waters (1996), An atmospheric tape recorder: The imprint of tropical tropopause temperatures on stratospheric water vapor, *J. Geophys. Res.*, *101*, 3989–4006, doi:10.1029/95JD03422.

Murphy, D. M., D. W. Fahey, M. H. Proffitt, S. C. Liu, K. R. Chan, C. S. Eubank, S. R. Kawa, and K. K. Kelly (1993), Reactive nitrogen and its correlation with ozone in the lower stratosphere and upper troposphere, *J. Geophys. Res.*, *98*, 8751–8773, doi:10.1029/92JD00681.

Newman, P. A., et al. (2002), An overview of the SOLVE/THESEO 2000 campaign, *J. Geophys. Res.*, *107*(D20), 8259, doi:10.1029/2001JD001303.

Niwano, M., K. Yamazaki, and M. Shiotani (2003), Seasonal and QBO variations of the ascent rate in the tropical lower stratosphere as inferred from UARS HALOE trace gas data, *J. Geophys. Res.*, *108*(D24), 4794, doi:10.1029/2003JD003871.

Oltmans, S. J., et al. (2001), Ozone in the Pacific troposphere from ozonesonde observations, *J. Geophys. Res.*, *106*, 32,503–32,525, doi:10.1029/2000JD900834.

Park, S., et al. (2007), The CO tracer clock for the Tropical Tropopause Layer, *Atmos. Chem. Phys.*, *7*, 3989–4000, doi:10.5194/acp-7-3989-2007.

Parodi, A., and S. Tanelli (2010), Influence of turbulent parameterization on high resolution numerical modeling of tropical convection observed during the TC4 field campaign, *J. Geophys. Res.*, doi:10.1029/2009JD013302, in press.

Peter, T., C. Marcolli, P. Spichtinger, T. Corti, M. B. Baker, and T. Koop (2006), When dry air is too humid, *Science*, *314*, 1399–1401, doi:10.1126/science.1135199.

Petropavlovskikh, I., et al. (2010), Low-ozone bubbles observed in the TTL during the TC4 campaign in 2007, *J. Geophys. Res.*, doi:10.1029/2009JD012804, in press.

Pfeilsticker, K., W. T. Sturges, H. Bosch, C. Camy-Peyret, M. P. Chipperfield, A. Engel, R. Fitzenberger, M. Muller, S. Payan, and B. M. Sinnhuber (2000), Lower stratospheric organic and inorganic budget for the Arctic winter 1998/99, *Geophys. Res. Lett.*, *27*, 3305–3308, doi:10.1029/2000GL011650.

Pfister, L., et al. (2001), Aircraft observations of thin cirrus clouds near the tropical tropopause, *J. Geophys. Res.*, *106*, 9765–9786, doi:10.1029/2000JD900648.

Pfister, L., H. B. Selkirk, D. O'C. Starr, P. A. Newman, and K. H. Rosenlof (2010), A meteorological overview of the TC4 mission, *J. Geophys. Res.*, doi:10.1029/2009JD013316, in press.

Randel, W. J., F. Wu, S. J. Oltmans, K. Rosenlof, and G. E. Nedoluha (2004), Interannual changes of stratospheric water vapor and correlations with tropical tropopause temperatures, *J. Atmos. Sci.*, *61*, 2133–2148, doi:10.1175/1520-0469(2004)061<2133:ICOSWV>2.0.CO;2.

Rosenlof, K. H., and J. R. Holton (1993), Estimates of the stratospheric residual circulation using the downward control principle, *J. Geophys. Res.*, *98*, 10,465–10,479, doi:10.1029/93JD00392.

Rosenlof, K. H., A. F. Tuck, K. K. Kelly, J. M. Russell, and M. P. McCormick (1997), Hemispheric asymmetries in water vapor and inferences about transport in the lower stratosphere, *J. Geophys. Res.*, *102*, 13,213–13,234, doi:10.1029/97JD00873.

Sayres, D. S., J. M. St. Clair, T. F. Hanisco, E. J. Moyer, A. S. O'Brien, J. B. Smith, E. M. Weinstock, J. G. Anderson, L. Pfister, and M. Legg (2010), Influence of convection on the water isotropic composition of the TTL and the tropical stratosphere, *J. Geophys. Res.*, doi:10.1029/2009JD013100, in press.

Scheuer, E., J. E. Dibb, C. Twohy, D. C. Rogers, A. J. Heymsfield, and A. Bansemer (2010), Evidence of nitric acid uptake in warm cirrus clouds during the NASA TC4 campaign, *J. Geophys. Res.*, *115*, D00J03, doi:10.1029/2009JD012716.

Schmidt, K. S., P. Pilewskie, B. Kindel, S. Platnick, M. King, G. Wind, G. T. Arnold, L. Tian, and M. Wendisch (2010), Apparent and real absorption of solar spectral irradiance in heterogeneous clouds, *J. Geophys. Res.*, doi:10.1029/2009JD013124, in press.

Schoeberl, M. R., A. R. Douglass, R. S. Stolarski, S. Pawson, S. E. Strahan, and W. Read (2008), Comparison of lower stratospheric tropical mean vertical velocities, *J. Geophys. Res.*, *113*, D24109, doi:10.1029/2008JD010221.

Schultz, M. G., et al. (1999), On the origin of tropospheric ozone and NO_x over the tropical Pacific, *J. Geophys. Res.*, *104*, 5829–5843, doi:10.1029/98JD02309.

Selkirk, H. B., H. Vömel, J. Valverde, and L. Pfister (2010), Detailed structure of the tropical upper troposphere as revealed by balloon sonde observations of water vapor, ozone, temperature and winds during the NASA TCSP and TC4 campaigns, *J. Geophys. Res.*, doi:10.1029/2009JD013209, in press.

Soden, B. J., I. M. Held, R. Colman, K. M. Shell, J. T. Kiehl, and C. A. Shields (2008), Quantifying climate feedbacks using radiative kernels, *J. Clim.*, *21*, 3504–3520, doi:10.1175/2007JCLI2110.1.

Staudt, A. C., D. J. Jacob, J. A. Logan, D. Bachiochi, T. N. Krishnamurti, and N. Poisson (2002), Global chemical model analysis of biomass burning and lightning influences over the South Pacific in austral spring, *J. Geophys. Res.*, *107*(D14), 4200, doi:10.1029/2000JD000296.

Staudt, A. C., D. J. Jacob, F. Ravetta, J. A. Logan, D. Bachiochi, T. N. Krishnamurti, S. Sandholm, B. Ridley, H. B. Singh, and B. Talbot (2003), Sources and chemistry of nitrogen oxides over the tropical Pacific, *J. Geophys. Res.*, *108*(D2), 8239, doi:10.1029/2002JD002139.

Strahan, S. E. (1999), Climatologies of lower stratospheric NO_y and O_3 and correlations with N_2O based on in situ observations, *J. Geophys. Res.*, *104*, 30,463–30,480, doi:10.1029/1999JD900775.

Takashima, H., and M. Shiotani (2007), Ozone variation in the tropical tropopause layer as seen from ozonesonde data, *J. Geophys. Res.*, *112*, D11123, doi:10.1029/2006JD008322.

Thompson, A. M., K. E. Pickering, D. P. McNamara, M. R. Schoeberl, R. D. Hudson, J. H. Kim, E. V. Browell, V. W. J. H. Kirchoff, and D. Nganga (1996), Where did tropospheric ozone over southern Africa and the tropical Atlantic come from in October, 1992? Insights from TOMS, GTE/TRACE-A and SAFARI-92, *J. Geophys. Res.*, *101*, 24,251–24,278, doi:10.1029/96JD01463.

Thompson, A. M., et al. (2003a), Southern Hemisphere Additional Ozonesondes (SHADOZ) 1998–2000 tropical ozone climatology: 2. Tropospheric variability and the zonal wave-one, *J. Geophys. Res.*, *108*(D2), 8241, doi:10.1029/2002JD002241.

Thompson, A. M., et al. (2003b), Southern Hemisphere Additional Ozonesondes (SHADOZ) 1998–2000 tropical ozone climatology: 1. Comparison with TOMS and ground-based measurements, *J. Geophys. Res.*, *108*(D2), 8238, doi:10.1029/2001JD000967.

Thompson, A. M., J. E. Yorks, S. K. Miller, J. C. Witte, K. M. Dougherty, G. A. Morris, D. Baumgardner, L. Ladino, and B. Rappenglueck (2008), Tropospheric ozone sources and wave activity over Mexico City and Houston during MILAGRO/Intercontinental Transport Experiment (INTEX-B) Ozonesonde Network Study, 2006 (IONS-06), *Atmos. Chem. Phys.*, *8*, 5113–5125, doi:10.5194/acp-8-5113-2008.

Thompson, A. M., et al. (2010), Convective and wave signatures in ozone profiles over the equatorial Americas: Views from TC4 (2007) and SHADOZ, *J. Geophys. Res.*, doi:10.1029/2009JD012909, in press.

Thornberry, T., K. D. Froyd, D. M. Murphy, D. S. Thomson, B. E. Anderson, K. L. Thornhill, and E. L. Winstead (2010), Persistence of organic carbon in heated aerosol residuals measured during TC4, *J. Geophys. Res.*, *115*, D00J02, doi:10.1029/2009JD012721.

Thuburn, J., and G. C. Craig (2002), On the temperature structure of the tropical substratosphere, *J. Geophys. Res.*, *107*(D2), 4017, doi:10.1029/2001JD000448.

Tian, L., G. M. Heymsfield, A. J. Heymsfield, A. Bansemer, L. Li, C. Twohy, and R. C. Srivastava (2009), A study of cirrus ice particle size distributions using TC4 observations, *J. Atmos. Sci.*, *67*, 195–216.

Vömel, H., et al. (2002), Balloon-borne observations of water vapor and ozone in the tropical upper troposphere and lower stratosphere, *J. Geophys. Res.*, *107*(D14), 4210, doi:10.1029/2001JD000707.

Vömel, H., D. E. David, and K. Smith (2007a), Accuracy of tropospheric and stratospheric water vapor measurements by the cryogenic frost point hygrometer: Instrumental details and observations, *J. Geophys. Res.*, *112*, D08305, doi:10.1029/2006JD007224.

Vömel, H., V. Yushkov, S. Khaykin, L. Korshunov, E. Kyrö, and R. Kivi (2007b), Intercomparisons of stratospheric water vapor sensors: FLASH-B and NOAA/CMDL Frost-Point Hygrometer, *J. Atmos. Oceanic Technol.*, *24*, 941–952, doi:10.1175/JTECH2007.1.

Wang, Y. H., et al. (2001), Factors controlling tropospheric O_3, OH, NO_x, and SO_2 over the tropical Pacific during PEM-Tropics B, *J. Geophys. Res.*, *106*, 32,733–32,747, doi:10.1029/2001JD900084.

Weisenstein, D. K., G. K. Yue, M. K. W. Ko, N. D. Sze, J. M. Rodriguez, and C. J. Scott (1997), A two-dimensional model of sulfur species and aerosols, *J. Geophys. Res.*, *102*, 13,019–13,035, doi:10.1029/97JD00901.

Wennberg, P. O., et al. (1998), Hydrogen radicals, nitrogen radicals, and the production of O_3 in the upper troposphere, *Science*, *279*, 49–53, doi:10.1126/science.279.5347.49.

Yost, C. R., P. Minnis, J. K. Ayers, D. A. Spangenberg, A. J. Haymsfield, A. Bansemer, M. J. McGill, and D. L. Hlavka (2010), Comparison of GOES-retrieved and in-situ measurements of deep convective anvil cloud microphysical properties during TC4, *J. Geophys. Res.*, doi:10.1029/2009JD013313, in press.

P. R. Colarco, S. R. Kawa, P. A. Newman, K. E. Pickering, S. Platnick, and D. O. Starr, Laboratory for Atmospheres, NASA Goddard Space Flight Center, Code 613, Greenbelt, MD 20771-0001, USA.

M. S. Craig, E. J. Jensen, L. Pfister, and M. F. Vasques, Earth Sciences Division, NASA Ames Research Center, MS 245-4, Moffett Field, CA 94035, USA.

K. W. Jucks and H. Maring, Earth Sciences Division, NASA Headquarters, Washington, DC 20546, USA.

M. J. Kurylo, Goddard Earth Sciences and Technology Center, NASA Goddard Space Flight Center, Code 610.6, Greenbelt, MD 20771-0001, USA.

G. G. Mace, Department of Atmospheric Sciences, University of Utah, Salt Lake City, UT 84112-0110, USA.

P. Minnis, Science Directorate, NASA Langley Research Center, Hampton, VA 23681, USA.

K. H. Rosenlof, Earth System Research Laboratory, NOAA, Boulder, CO 80305, USA.

M. R. Schoeberl, Polar Office, Science and Technology Corporation, 10005 Old Columbia Rd., Columbia, MD 21046, USA.

H. B. Selkirk, Goddard Earth Sciences and Technology Center, NASA Goddard Space Flight Center, Code 613, Greenbelt, MD 20771-0001, USA.

O. B. Toon, Department of Atmospheric and Oceanic Sciences, University of Colorado at Boulder, Campus Box 392, Boulder, CO 80309-0392, USA. (toon@lasp.colorado.edu)

P. O. Wennberg, Division of Engineering and Applied Sciences, California Institute of Technology, MS 150-21, Pasadena, CA 91125, USA.

S. C. Wofsy, Department of Earth and Planetary Sciences, Harvard University, Pierce Hall 110D, Cambridge, MA 02138, USA.